THESIS

MULTI-SCALAR RESPONSE OF AN EXPERIMENTAL FIXED-WALL MEANDERING CHANNEL TO A SEDIMENT SUPPLY INCREASE

Submitted by

David Cortese

Department of Civil and Environmental Engineering

In partial fulfillment of the requirements

For the Degree of Master of Science

Colorado State University

Fort Collins, Colorado

Fall 2020

Master's Committee:

Advisor: Peter Nelson

Ryan Morrison
Ellen Wohl

ABSTRACT

MULTI-SCALAR RESPONSE OF AN EXPERIMENTAL FIXED-WALL MEANDERING CHANNEL TO A SEDIMENT SUPPLY INCREASE

Meandering river planforms are prevalent and well-studied features in the natural landscape. These rivers commonly exhibit a characteristic morphology of fine-grained point bars along the inner banks of meander bends with coarser pools along the outer banks. If subjected to a change in sediment supply, these rivers are likely to respond at various spatial and temporal scales through adjustments to sorting patterns, cross-sectional shape, and reach-scale morphology. In this study, a flume experiment was conducted to document the temporal progression of responses across scales of a fixed-wall meandering channel to a sediment supply increase. The 0.344 m wide experimental channel consisted of four meander bends following a sine-generated trace with a 20-degree crossing angle, meander wavelength of 2.75 m, and a unimodal sediment mixture with median grain size of 0.62 mm. The channel was provided constant flow and sediment supply until an initial equilibrium was established, after which the sediment supply was doubled until a new equilibrium state was reached. The experimental channel developed characteristic bar-pool morphologies and sorting patterns with superimposed, mobile, scaled gravel-dune bed forms during both phases of the experiment. After the sediment supply increase, dynamic adjustments occurring from smaller to larger scales took place. Initially, the dunes essentially disappeared, after which the relief of the bars decreased. Both of these sub-reach-scale responses were temporary, however, and ultimately the dunes and bar-pool morphology returned to their conditions at the beginning of the sediment supply increase. The

long-term and largest-scale response to the supply increase was a 44% increase in bed slope. To explain these observations, we propose a conceptual model wherein the channel undergoes a temporal progression of responses from smaller to larger spatial scales, with the total response potential at each scale related to the conditions and constraints at that scale. This conceptual understanding allows us to reconcile seemingly divergent outcomes from previous research on how meandering rivers adjust to sediment supply changes.

ACKNOWLEDGEMENTS

I would like to thank my advisor Dr. Peter Nelson for providing me the opportunity to work with him on this research project and for his thoughtful perspective and guidance throughout my time at Colorado State University, returning to graduate school has been all I could have hoped for and more. Thank you to my committee members, Dr. Ellen Wohl and Dr. Ryan Morrison, for their constructive input regarding this work and for their wonderful classes which I thoroughly enjoyed.

To my wife Nika, thank you for your constant love and support and for being adventurous in moving halfway across the country to Fort Collins so I could return to school. To our dog Zena, thanks for always making sure I remembered to take breaks from thesis writing to take you on walks, you never forgot. Thank you to my parents and brother for always being supportive and believing in me, and for tolerating me talking about the intricacies of conducting a flume experiment more than the average person should probably have to. Lastly, I would like to thank Ryan Brown, Danny White, Nick Brouillard, Beau Van Der Sluys, Ben Tyner, and Taylor Hogan for their assistance, comradery, and friendship both in and out of the lab.

TABLE OF CONTENTS

LIST OF TABLES

LIST OF FIGURES

NOTATION

BP_a	Mean bar-pool amplitude
BP_w	Mean bar-pool wavelength
D_a	Mean dune amplitude/height
D_w	Mean dune wavelength
H_m	Reach-averaged depth
Q_b	hourly-averaged bed load transport
S_b	Reach-averaged bed slope
S_v	Valley slope
S_w	Reach-averaged water surface slope
d_{50}	Median grain-size diameter
$f_{bp}{}''$	Within-channel resistance attributed to bar-pool bed forms
$f_d{}''$	Within-channel resistance attributed to dune bed forms
k_s'	Roughness height, assumed to be equal to surface d_{50}
τ_*	Dimensionless boundary shear stress
τ_{*c}	Dimensionless critical shear stress for incipient motion, assumed to be 0.03
D	Depth
M	Total streamwise distance for a single meander
R	Hydraulic Radius
W	Width
Y	Flow depth

f'	Grain-scale resistance to flow
f''	Within-channel resistance to flow
f'''	System wide resistance to flow due to sinuosity
$fsys$	Total system resistance to flow
g	Acceleration due to gravity
s	Streamwise distance along a single meander
u	Mean flow velocity
φ	Deviation angle of the trace from the down valley direction
ω	Maximum angle deviation from the down valley direction

1 Introduction

Meandering rivers are widely prevalent and well-studied features in the natural landscape. These rivers commonly exhibit a characteristic morphology of point bars composed of fine sediments along the inner banks of meander bends and coarse sediment pools along the outer banks (Bridge, 1977; Gary Parker & Andrews, 1985; Dietrich & Whiting, 1989; Whiting & Dietrich, 1991). This bar-pool morphology reflects a balance of flow and sediment transport in curved channels. Channel curvature induces helical flows and spatial variations in boundary shear stress (Dietrich & Smith, 1983; Dietrich & Whiting, 1989) which along with topography-induced gravitational forces gives rise to the observed sorting patterns of coarse sediments in pools and fine sediment on bars in meandering channels (Bridge, 1977; Gary Parker & Andrews, 1985; Dietrich & Whiting, 1989; Whiting & Dietrich, 1991; Clayton, 2010). These sorting patterns and the tendency to route coarse sediments through the pools and fines toward the bars are believed to help maintain and stabilize bar-pool morphology under conditions of dynamic equilibrium (Whiting & Dietrich, 1991; Clayton & Pitlick, 2007).

It has long been understood that streams will respond to changes in hydraulics and sediment supply (Gilbert, 1917; Mackin, 1948; Lane, 1955; Schumm, 1968). Efforts to understand what determines a channel's equilibrium condition have produced a variety of explanations and theories such as Lane's balance, the concept of the graded river, and extremal hypotheses (e.g., minimum stream power, maximum friction factor, principle of least action) (Mackin, 1948; Lane, 1955; Chang, 1979; Davies & Sutherland, 1983; Huang & Nanson, 2000). Eaton et al. (2004) further proposed a rational regime model whereby a channel achieves equilibrium by maximizing the total resistance of the system, where the resistance is defined as:

$$fsys = f' + f'' + f'''$$ (1)

where $fsys$ is the total resistance of the alluvial system, f' is the grain resistance, f'' is the within-channel resistance such as dunes, bars, and other types of in-channel features, and f''' is the reach-scale form resistance due to channel sinuosity. According to this model, discharge, sediment supply, and valley gradient are identified as the dominant independent variables to which an alluvial system will respond though adjustments to one or more of the components of total system resistance.

The specific manner in which an alluvial system will respond, however, has been observed in field and flume studies to come in many different forms. Braudrick (2013), and references therein, summarized six ways that a channel can respond to a sediment supply increase: 1) a fining of the bed sediments, 2) shoaling of pools, 3) bar growth into pools thereby decreasing cross-sectional relief, 4) slope increase by aggradation of the bed, 5) channel planform changes such as straightening, avulsions, or cutoffs, and 6) active channel width changes that occur faster than the depth declines. Buffington (2012) summarized channel adjustments as a series of "successive, overlapping, spatial and temporal scales of morphologic response," that included grain-scale adjustments, bed form adjustments, altered channel geometry, and finally altered stream gradient (Figure 1). In this framework, he described the potential for a "progression of successive scales of response" depending on the geomorphic work conducted by a competent flow event and the time necessary for a given scale of response to occur (Wolman & Miller, 1960; Buffington, 2012). These temporal and spatial relationships between channel response mechanisms to sediment supply changes have, to our knowledge, not been documented in flume experiments for meandering channels.

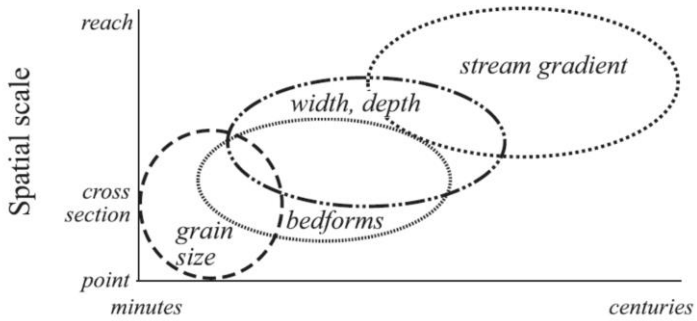

Figure 1 Reproduction from Buffington (2012), after Knighton (1998): Spatial and temporal scales of channel response variables in alluvial rivers

There have been a number of field and flume studies that have documented the effects of sediment supply on bed surface sorting patterns (Dietrich et al., 1989; Lisle et al., 1993; Buffington & Montgomery, 1999; Nelson et al., 2009), riffle pool morphology (Lisle, 1982; Lisle & Hilton, 1992; Lisle & Madej, 1992; Wohl & Cenderelli, 2000; Rathburn & Wohl, 2003), alternate bars (Lisle et al., 1993; Cui et al., 2003; Nelson et al., 2010; Venditti et al., 2012; Podolak & Wilcock, 2013; Bankert & Nelson, 2018), variable-width channels (Nelson et al., 2015; Brew et al., 2015; Morgan, 2018) and meander migration (Constantine et al., 2014). These studies have shown bed surface patchiness and grain size to be directly affected by changes in sediment supply, with a coarsening of the bed occurring in response to a decreased supply and a fining of the bed to an increase in supply. In an experiment in a straight flume, Venditti et al. (2012) found that termination of upstream sediment supply caused alternate bars fixed in place by a channel constriction to be stripped out in place via erosional processes, while alternate bars that formed and stabilized under sediment feed conditions began to migrate downstream leaving behind a plane bed. This differed from the observations of Lisle et al. (1993) who reported that decreased sediment supply in a straight flume with alternate bar bed forms led to a coarsening of

the bed, incision of the thalweg, and ultimately an emergence of the alternate bars under a significantly reduced sediment supply.

Field studies of riffle-pool morphology have shown deposition of sediment in pools in response to prescribed reservoir sediment releases (Wohl & Cenderelli, 2000; Rathburn & Wohl, 2003), dam removals (Brew et al., 2015), and flood induced landslides (Lisle, 1982). Cui et al. (2003) found that sediment pulses temporarily subdued cross-sectional relief and alternate bars in straight-walled flume experiments on high-gradient mountain streams. Studies have shown that sediment pulses comprising materials finer than the bed sediment increased the mobilization of coarse grains (Cui et al., 2003; Venditti et al., 2010a, 2010b), while coarser pulses left bed armor layers unaffected (Cui et al., 2003). Additionally, Cui et al. (2003) observed that the degree to which alternate bar relief was subdued by a sediment pulse was related to the relative differences between the bed material grain size and the pulse sediments. Similarly, a field study by Madej (2001) also found that sediment pulses had the short-term effect of decreasing channel roughness and structure, indicating decreased relief, and that those effects decrease over time with the number of mobilizing flow events. In flume studies investigating the effects changing sediment supply on straight, variable-width channels, Nelson et al. (2015) found that an increase in the slope was the main response to a doubling in sediment supply under constant flow rates and Morgan's (2018) unsteady-flow experiments found that the primary response to a sediment supply increase was a reduction in relief between riffles and pools rather than a significant slope increase.

For meandering rivers, only a few flume studies have investigated the effects of sediment supply on bar-pool morphology and sediment sorting (Eaton & Church, 2004, 2009; Erwin, 2013; Braudrick, 2013). Eaton and Church (2004) performed a series of stream table experiments

studying equilibrium conditions for scaled gravel-bed meandering channels under varying sediment supply conditions where the channel bed and banks were free to adjust. In their study, they found that slope change was the dominant adjustment response as their channels approached equilibrium through vertical degradation and lateral erosion of bank materials. Eaton and Church (2009) further investigated the effects of sediment loading on meandering channels with a fixed-wall condition and found that a doubling of the sediment supply could largely be accommodated by grain-scale changes to the surface sorting on the bed with little effect on slope. Erwin (2013) conducted a field-scale study of a point bar and pool at the St. Anthony Falls Laboratory at the University of Minnesota and observed that a 5-fold increase in sediment supply caused changes to the cross-sectional relief via shoaling in the pool and a lateral widening of the point bar into the pool. Braudrick (2013) observed changes to a scaled meandering channel with fixed walls and nine bends of varying curvature to a doubling in sediment supply and found that a slope increase via aggradation was the primary response, along with a decrease in the spatial extent of coarse facies and an increase in finer facies, with little change to bar-pool morphology. His investigations concluded that the amount of aggradation experienced by the channel would likely have caused avulsion or cutoff in a real-world setting. These somewhat contradictory observations highlight the need for additional research to improve our understanding of the mechanisms by which meandering channels will respond to changes in sediment supply, as well as the possible temporal progression of potential responses.

In this paper, we aim to better understand the temporal progression of the geomorphic response of meandering gravel-bed rivers to sediment supply increases. We present results from an experiment in a fixed-wall meandering flume in which we developed dynamic equilibrium, then doubled the sediment supply and documented the response. Our work seeks answers to the

following questions: 1) to what extent does increased sediment supply alter the sorting, bar-pool morphology, and equilibrium slope in a fixed-wall meandering channel experiencing an increased sediment supply; and 2) what is the temporal progression of the scale of response in meandering channels undergoing an equilibrium shift? Further, during our experiments we observed development of scaled gravel-dune bed forms which raised an additional question: 3) to what extent do gravel dunes respond to an increase in sediment supply in bed load-dominated meandering channels? In our experiment, small-scale changes at the scale of individual cross-sections and meanders constituted the initial response, but these were temporary and ultimately overwhelmed by a large-scale slope increase. Our results suggest a conceptual understanding of meandering river response to sediment supply increases, wherein the channel undergoes multiple spatial and temporal scales of response that occur simultaneously over different time-scales and that dynamically interact.

2 Methods

2.1 Experimental Overview

The results presented herein are from an experiment conducted at the Engineering Research Center Hydraulics Laboratory at Colorado State University. In these experiments, a scaled gravel-bed meandering channel with fixed walls was observed under conditions of constant flow rate at two sediment supply rates in order to observe the effect of increased supply on a meandering channel. First, a dynamic equilibrium was established (Equilibrium 1) by operating the flume with an initial sediment supply, starting from a flat screeded bed, to allow for self-generated bar-pool morphologies to develop. Dynamic equilibrium conditions were determined from observations of averaged water-surface slopes, bed slopes, and bed load

transport rates. Once this equilibrium was achieved, the sediment supply was doubled and detailed measurements were collected to record the response of the channel until it reached a new equilibrium condition (Equilibrium 2). In this paper the duration of the experiment up until Equilibrium 1 is referenced as Run 1, and the duration of the experiment where the channel transitions from Equilibrium 1 to Equilibrium 2 is referred to as Run 2.

2.2 Experimental Design

The experimental conditions were selected to create a generic, scaled, meandering river model with hydraulic conditions and transport processes representative of those found in meandering gravel-bed rivers. The flume width, slope, flow rate, and bulk sediment grain size were selected such that a bed of mixed sand with a median grain size (d_{50}) of 0.62 mm would predominately be transported as bed load with a flow strength sufficient to fully mobilize the range of bed sediments. This was accomplished using a target ratio of the dimensionless boundary shear stress τ_*, to dimensionless critical boundary shear stress τ_{*c}, equal to 2, where τ_{*c} was assumed to be 0.03 for the sediments used in this experiment (Wilcock & McArdell, 1993). The flume design also sought to replicate a width-to-depth (W/D) ratio of 20, with a bed slope of 0.005, which are conditions typical of many gravel-bed rivers (Braudrick, 2013). Using a scaling factor of 1/50 (following the methodology of Parker et al., 2003), our flume corresponds to a field prototype with a d_{50} of 31 mm, width of 17 m, and flow rate of 35.3 $\frac{m^3}{s}$, which are characteristic of meandering gravel-bed rivers summarized in a database compiled by Braudrick (2013). Normal depth calculations were used to select the flow rate and initial bed slope and the Wilcock and Crowe (2003) bed load transport relation was used to estimate the initial sediment supply.

The planform geometry of the experimental channel was broken up into 6 sections: a straight entrance section, 4 bends (Meanders 1-4), and a straight exit section (Figure 1). Each meander section had a wavelength of 2.75 m and a wavelength-to-width ratio of 8, which resulted in a channel width of 0.344 m. The centerline of the meander sections was described using a sine-generated trace (Langbein and Leopold, 1966) as described by:

$$\varphi(s) = \omega \sin\left(\frac{s}{M} 2\pi\right) \quad (2)$$

where φ is the deviation angle of the trace from the down-valley direction, ω is the maximum radian angle deviation from the down-valley direction, s is the streamwise distance along a single meander, and M is the total streamwise distance for a single meander. For this experiment ω was set to 0.349 radians, or 20 degrees.

2.3 Experimental Construction

The experimental channel was constructed within a larger 1.22-m-wide by 18-m-long flume (Figure 2) using a 3/4" marine plywood base and 1/8" acrylic sheeting for the channel sidewalls. The meandering planform of the channel was cut into the plywood base using laser cut templates and a router to form grooves into which the acrylic walls were secured using silicone caulking. At the upstream end, a headwall and weir were constructed to direct flow from the larger flume headbox into the upstream end of the inset meandering channel and similarly, a plywood sediment weir and flood wall was constructed at the downstream to serve as an elevation control point and facilitate filling of the flume.

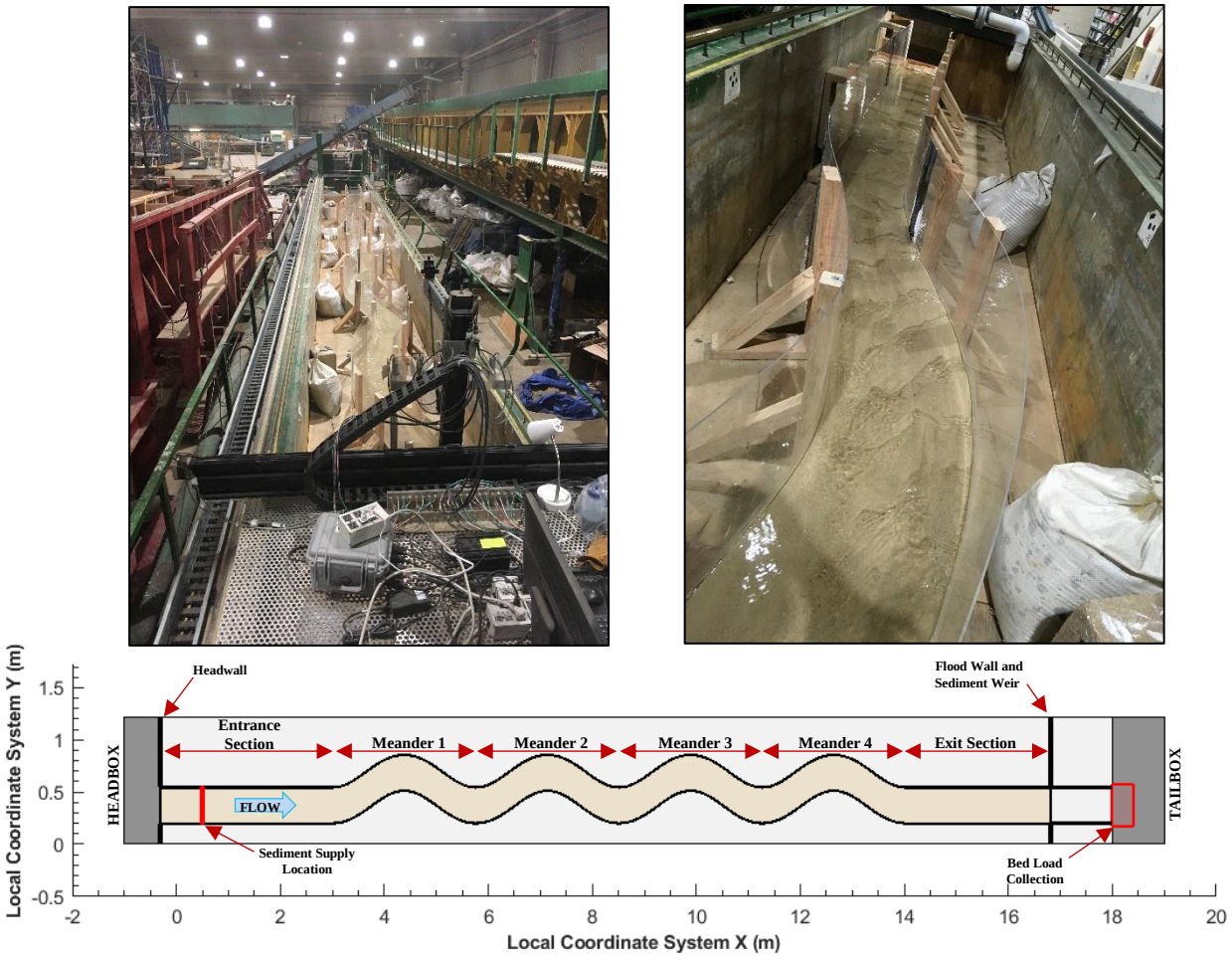

Figure 2 Experimental channel overview (bottom), with view looking downstream (upper left) and upstream (upper right).

The flume was filled with a sediment mixture ranging in size from 0.0125 to 2.8 mm with a median grain size of 0.62 mm (Figure 3). The sediment was placed into the flume while slightly damp to reduce the likelihood of vertical grain sorting during placement, and the bed was smoothed and screeded to a relatively planar surface with an initial slope of approximately 0.005. The bed was tamped down by hand but was not compacted. A gravel-filled sandbag was placed just downstream of the headbox weir to provide scour protection as the flow entered the flume from the headbox.

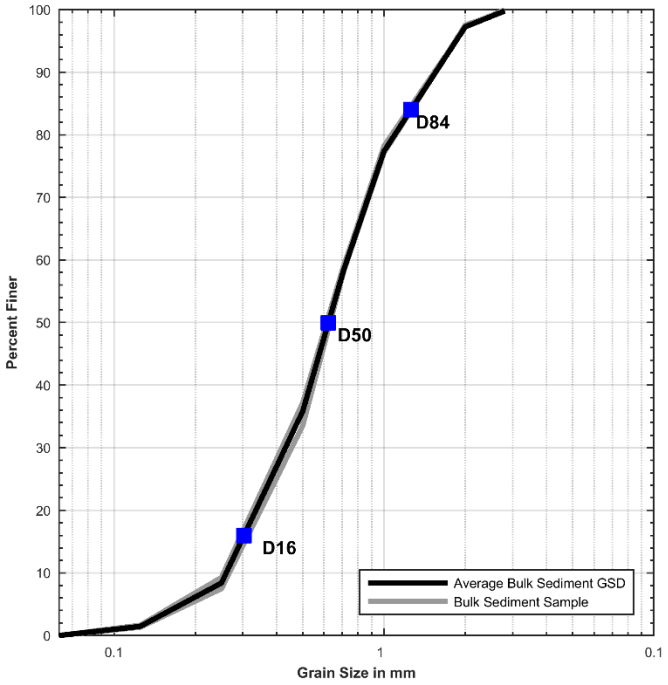

Figure 3 Bulk sediment grain-size distribution

Water supply for the experiment was delivered through a three-inch firehose connection to a large supply pipe from the nearby Horsetooth Reservoir. A manifold system was constructed at the flume with a three-inch globe valve and gate valve to facilitate turning flows on and off as well as for fine flow adjustments throughout the course of the experiment. Flow monitoring was accomplished using a Badger M2000 electronic flow meter, set to display with a Damping Factor of 20 seconds with a reported accuracy within 0.2% of the flow rate.

2.4 Experimental Procedure

Both Run 1 and Run 2 were conducted using a constant flow rate of 2.0 l/s and differed only in the sediment supply rate applied to the upstream end of the flume. The sediment supply was added to the flume manually, every 5 minutes, by spreading prefilled containers of the bulk sediment uniformly across the channel 0.5 m downstream from the inlet (Figure 2). During Run 1 the sediment supply was 20 g/min added in 100 g increments; in Run 2 the supply was 40

g/min added in 200 g increments. Containers were prefilled periodically during the runs using a laboratory scale with accuracy of ± 0.01 g.

Run 1 proceeded until quasi-equilibrium conditions were achieved (described in Section 3.1), a duration of 80.1 hours (80 hours and 5 minutes), at which point Run 2 began and proceeded until a new quasi-equilibrium was established, a duration of an additional 150 hours. During Run 2, the flume was run in daily increments usually lasting 10 hours, while run times varied more during Run 1 while developing measurement methodologies. Between these daily increments, detailed topographic measurements of the bed were collected to document the evolution of the channel (see Section 2.5). After Run 2, there was a 20 hr period where the flume was run with no sediment supply to confirm experimental methodologies during which limited measurements were recorded.

At the beginning of each day the flume was filled with water from the downstream end until the bed was fully submerged prior to turning on the full flow rate. This procedure was adopted during Run 1 to limit disturbances while filling the flume due to the small grain size of the bed material and the bar-pool morphology that developed. A scour hole that formed at the inlet to the entrance section was also filled separately to prevent significant erosion from downstream-filling water. This method of start-up caused only minor erosional impacts to the downstream end of the pools when water first began to spill into the empty pools and to dune bed forms as water first overtopped dune crests. These impacts were monitored each day and were typically not visible at the time of the first bed observation, usually 15 minutes after starting the full flow rate each day. Once the flume bed was submerged, the prescribed 2.0 l/s flow rate was turned on and the tailbox gate was gradually lowered to slowly increase the velocities in the flume until water freely spilled over the sediment weir at the tailbox.

A variety of measurements were collected throughout each daily segment of the experiment. These measurements have been summarized in Table ***1*** and are described in further detail in subsequent sections.

Table 1 Experimental measurement overview and sampling frequency

Type of Measurement	Description of Sampling Method	Typical Frequency (during Run 2)	Additional Info
Topography	Photo collection for Structure-from-Motion photogrammetry.	Every 10 hours of flume run time	Section 2.5
Bed Load Sampling	Bed load sediment collection in tailbox using milk crates lined with fine mesh bags.	Every hour	Section 2.6
Sediment Supply Sampling	Collection of sediment from the bulk mix providing the supply.	1-3 samples per day	Section 2.6
Water Surface Elevation	Profile generated from 5 ultrasonic sensors connected to a computer-controlled measurement cart.	Every 0.5 hours	Section 2.7
Dune Observation Sketches	Sketches were drawn denoting the spatial coverage of dune bed forms and other observations of interest.	Every 0.5 hours	Section 2.13
Facies Mapping	Hand-drawn facies map of observed sediment sorting patterns using visual observations, orthophotos, and DEM topography.	End of Run1 and end of Run 2	Section 2.8
Surface Sediment Sampling	Grease block sampling of sediment facies types	End of Run 1 and end of Run 2	Section 2.9

2.5 Structure-from-Motion (SfM) Modeling

Bed topography was measured using structure-from-motion photogrammetry using methodology similar to that described in Morgan et al. (2017) and which generally followed the procedures of USGS National UAS Project Office (2017). Photos of the bed were taken after the bed had drained and dried, typically on the day following a run segment. A Canon Rebel T3i DSLR camera with an EF-S 24mm prime lens was mounted to a computer-controlled

measurement cart that moved along rails traversing the length of the flume. The upstream portions of the flume were unable to be photographed from the cart from all angles, so supplemental photos were taken using a tripod positioned along the flume walls. Multiple camera angles were used to ensure that the flume bed was captured in photos with sufficient overlap due to the meandering planform and translucent acrylic walls; including facing up/down the flume (40 degrees from horizontal), perpendicular to the bed (90 degrees downward), and angles aimed toward the center of the flume taken from the each side of the flume walls. As described in Morgan et al. (2017), it is difficult to quantify a percentage overlap when using multiple camera angles in a flume, therefore, we adapted our photograph collection strategy until we achieved satisfactory modeling results during preliminary tests and consistently had greater than 9 photographs covering every portion of the flume bed.

Two sets of photographs were taken during each topographic measurement during Run 2, used to generate two types of photogrammetric products for this study. One set was composed of approximately 500 photos which captured the floor, walls, and wall tops of the flume as well as the inset meandering channel planform. This set of photographs also captured 8 georeferenced targets, set along the tops of the flume walls, which were used to transform the SfM model to the local flume coordinate system and to assess the accuracy of each SfM dataset. This photo set was processed in Agisoft Metashape at “medium” quality to produce a three-dimensional topographic point cloud. Average RSME error for the topographic datasets was 0.0013 m. A second set of approximately 350 photos was also collected, taken perpendicular to the flume bed, at a much closer distance of about 0.35 m to 0.38 m above the bed. This second set of photos was processed into an “ultra-high” quality point cloud of only the flume bed, a detailed orthophoto, and ultra-high-resolution digital elevation model (DEM) with a cell size of 0.083 mm (145

pix/mm^2). The ultra-high-resolution DEM captured grain-scale roughness elements for the coarser size fractions of the bed sediment and met criteria proposed by Morgan (2017) for using SfM to capture grain-scale topography for particles > 0.68 mm with greater than 100 pixels per particle.

2.6 Sediment Supply and Bed Load Sampling

Samples of the sediment supply were collected by setting aside 1-2 containers of the pre-measured bulk sediment throughout each day the flume was run. Typically, these samples came from the start of the day, end of the day, or at times where a new batch of bulk sediment was being pre-weighed into containers. Samples were sieved and weighed to obtain grain-size distributions and confirm that a consistent sediment supply was maintained throughout the experiment.

All sediments transported through the flume were collected in the tailbox by diverting flows and sediments into a plastic milk crate fitted with a fine mesh nylon bag with an opening size of 0.125 μm. Preliminary testing of this collection method indicated that approximately 3 percent (by weight) of the finest sediments were lost through flushing out of the mesh openings. Two crates with bag liners were alternately swapped each hour to provide hourly-averaged bed load samples. Each time the crates were alternated, the bag was emptied and the sediment collected was oven dried, weighed, and bagged. Samples were later sieved to obtain grain-size distributions of the bed load at five-hour intervals throughout the duration of the experiment.

2.7 Water Surface Measurements

Water surface measurements were collected by scanning the flume using five Massa ultrasonic sensors mounted on the flume cart. Software was used to control and record the position of the cart, sensors, and sensor readings during each scan. Water surface scans typically

consisted of 5 passes along the flume, resulting in 25 longitudinal profiles with an average lateral spacing of approximately 5 cm or less, and each scan took approximately 15 minutes to complete. The data were processed in MATLAB® to: 1) exclude sensor readings outside of the meandering flume walls, 2) filter out erroneous sensor readings that bounced off the flume walls, and 3) apply a calibration offset developed to adjust for subtle bends in the brass rails that the cart uses to traverse the flume. The filtered elevations were transformed into streamwise s and n coordinates, where s is the streamwise stationing and n describes the transverse coordinate (Smith & Mclean, 1984; Legleiter & Kyriakidis, 2007). Water surface elevations were then plotted by their s coordinate and smoothed with a robust quadratic regression line to generate an estimate of the continuous water surface. Therefore, water surface elevations reported should be considered a representation of the mean water surface elevation at any cross section. Due to the low velocities anticipated in this experiment, super elevation of the water surface around meanders was not anticipated nor likely measurable with the accuracy of the Massa sensors (RSME = 0.0003 m).

2.8 Hand-Drawn Facies Mapping

Sediment sorting patterns were recorded at the end of Runs 1 and 2 using hand-drawn maps. The bed was divided into course, medium, and fine facies types characterized as follows: 1) coarse patches consisting primarily of coarse sediments with readily discernable grain sizes (d_{50} ~ 0.81 mm), visible voids, and few to no fine surface sediments, 2) medium patches consisting of fine and coarse sediments with a nearly homogeneous texture or consisting of fines embedded with larger discernable particles and sparse texture (d_{50} ~ 0.51 mm), with few to no visible voids, and 3) fine patches consisting of nearly all fines with a homogenous texture (d_{50} ~ 0.36 mm), few to no large discernable grains, and grainsizes small enough that the observer

cannot readily identify individual grains. The maps were created digitally by drawing shapefile outlines onto an orthophoto of the flume bed. Direct observations of the bed, the orthophoto, and high-resolution DEM were all used in conjunction for the generation of the facies maps.

2.9 Surface Sediment Sampling

The sediment facies types delineated on the hand-drawn facies maps for Equilibriums 1 and 2 were further characterized through physical surface sampling using a grease block technique (Ingle, 1966; Bunte & Abt, 2001). To the extent practicable, sample locations of all facies types spanned the length of the flume such that each facies type was sampled twice per meander wavelength with one sample located in the entrance and exit sections of the flume, for a total of 10 samples per facies type.

Sampling was conducted using a 3.5-cm square of cardboard coated in petroleum jelly to a thickness that allowed the largest surface particles to become imbedded when applied with pressure to the bed. Care was taken to try not to remove subsurface layers, but due to the fine grain size and moisture content of the bed sediments, some subsurface grains were also removed due to clumping. In these cases, light brushing was used to remove obvious subsurface sediments while leaving the layer affixed to the petroleum jelly undisturbed. The cardboard sampling squares were then rinsed with hot water into cups containing a mixture of hot water and dish detergent to separate the sediment sample from the cardboard and petroleum jelly; oils from the melted petroleum jelly floated on the water surface while sediments settled to the bottom. The mixtures were then decanted several times with additional hot water and dishwashing detergent to fully separate the sediment grains. Samples were later oven dried and sieved obtain area-by-weight grain-size distributions. Reported distributions have been converted into a grid-by-number distribution using the method of Marion and Fraccarollo (1997), developed for similar

surface wax sampling, for easy comparison with the bulk sediment sample distributions, reported as volume-by-weight (Bunte & Abt, 2001).

2.10 Topographic Dataset Processing

The medium-quality point clouds generated for topographic analysis were post-processed using the open-source CloudCompare software package (*CloudCompare*, 2020). Point clouds were filtered to a 2 mm point spacing, which reduced the size of the cloud from approximately 50 million to 10 million points. The point clouds were then clipped to extract the meandering bed surface from the rest of the flume and filtered with a Statistical Outlier Removal (SOR) filter. Additional manual point removal was used to clean the clipped clouds to remove portions of the flume walls that remained within the clipping boundary. The cloud was then exported and gridded using Surfer® 13 by Golden Software, LLC into a 5 mm grid using a kriging method for analysis in MATLAB®. MATLAB® was used to transform the gridded data into s and n coordinates (Legleiter & Kyriakidis, 2007) and detrend the data by subtracting a least-squares linear fit of the average cross-sectional bed elevations (the mean of unique n elevations) from the raw gridded elevations.

2.11 Spectral Analysis Bed Form Separation

Two scales of bed forms became evident throughout the experiment: 1) bar-pool morphology forced by the meandering planform of the channel and 2) spatially and temporally varied dune bed forms superimposed over the underlying topography. This posed a challenge to making inferences regarding channel response directly from the gridded topographic data sets. For example, large topographic differences in a cross-section could easily be misinterpreted as rapid changes to the bar height rather than a transient dune moving downstream. To better understand the channel response at each of these spatial scales, a spectral analysis procedure was

applied to our topographic datasets to extract and separate the two types of bed form features. Spectral analysis has been applied to study patterns of multiple spatial scales in topography (Perron et al. 2008) and has wide application for the analysis of dune morphology (van Dijk et al., 2008; Lisimenka & Kubicki, 2017; Wang et al., 2019, 2020).

Similar to a bandpass filter used for signal processing, spectral analysis can be utilized to filter topography based on the wavelength, or actual length of a physical feature. The spectral analysis was used to separate the long undulating bar-pool features from the relatively short-wavelength dunes. Our analysis applied a 1-D spectral analysis filtering procedure, similar to those found in Perron et al. (2008) and Wang et al. (2019), to each streamwise profile in our detrended topographic grids (Young, 2020). The topographic grids were first broken up into a collection of 1-D streamwise profiles according to their transverse *n* coordinate. Then, each profile was: 1) transformed using a Fast Fourier Transform (FFT) into the frequency domain, 2) filtered with a Gaussian weighted mask to smoothly remove wavelengths less than 2 m (Perron et al., 2008), 3) transformed out of the frequency domain using an inverse FFT, and 4) recombined with all of the processed 1-D filtered profiles of the original gridded data.

The result of this process was a "low-pass" filtered topographic grid representing physical features that were larger than 2 m in length in the streamwise direction (Figure 4). In this experiment the bar-pool wavelength was the same order of magnitude as the meander wavelengths, roughly 2.75 m, and was therefore retained in the low-pass filter. The low-pass filtered elevation grid was then subtracted from the original unfiltered elevation data to obtain a "high-pass" topographic grid of only the physical features smaller than 2 m, which contained all of the shorter-wavelength dune bed forms. Because our analysis only sought to separate out long undulating bar-pool features from the smaller dune bed forms, a 1-D spectral analysis in the

streamwise direction was sufficient to achieve our needs in lieu of a 2-D spectral analysis procedure.

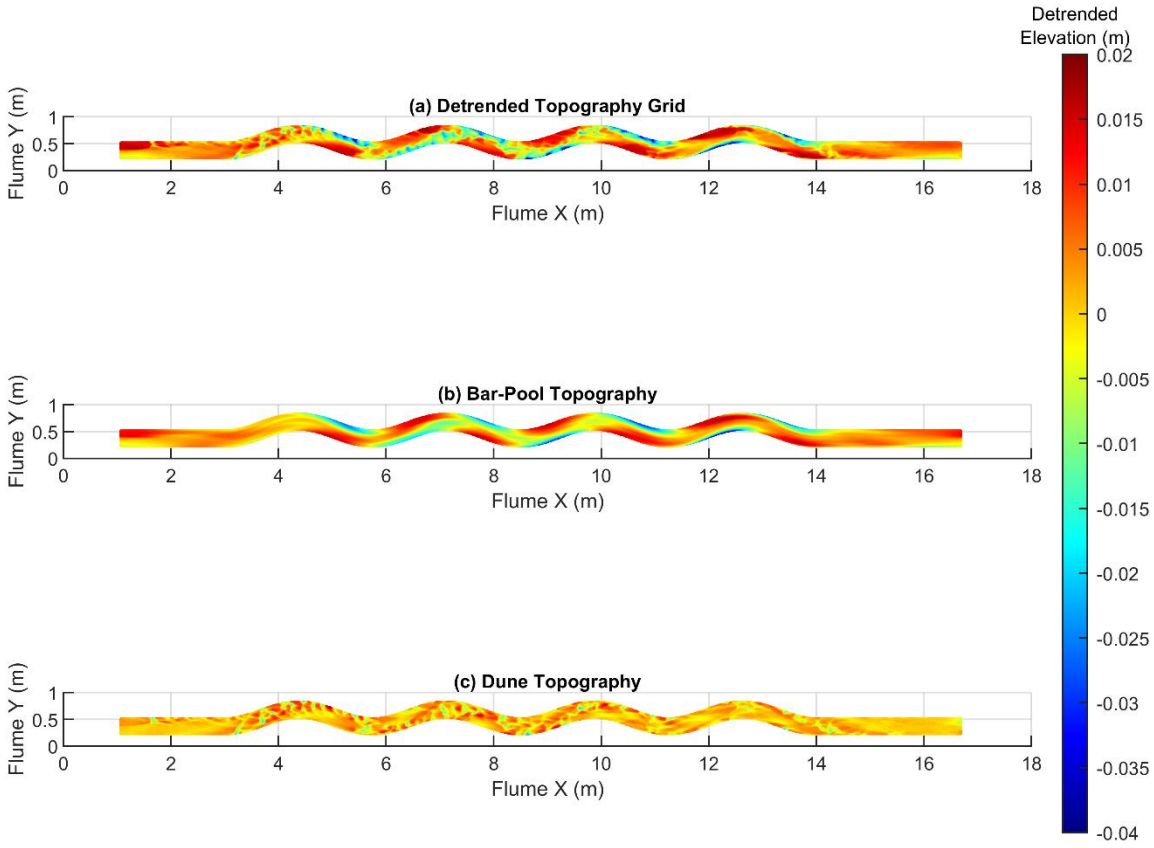

Figure 4 Example of spectral analysis procedure. (a) Shows the detrended topography gridded data before the analysis. (b) Shows the extracted low-pass bar-pool topography. (c) Shows the extracted high-pass dune topography. If the extracted topographic grids are summed, the result is the original detrended grid (i.e., (a) = (b) + (c)).

2.12 Zero-Crossing Analysis

The 5-mm low-pass and high-pass topographic grids were used to characterize the geometric characteristics of the bar-pool morphology and the dunes observed during the experiments. We used a zero-crossing analysis similar to van der Mark et al. (2008) and Nelson and Morgan (2018). For the low-pass topographic grids containing bar-pool topography, 1-cm strips of the left and right (in (*s*, *n*) space) portions of the grid, corresponding to topography near the left and right channel walls, were first subtracted to create a profile of elevation differentials (Figure 5b). The points where the profile crossed the zero line (zero-crossing) were then

identified and used to locate local maxima and minima between adjacent zero-crossings, which were identified as bar tops and pool bottoms, respectively. Bar-pool amplitudes were defined as the elevation difference between a bar top and the downstream pool bottom and bar-pool wavelengths were defined as the distance between two subsequent bar tops. For each data set, calculated bar-pool characteristics were averaged for the middle 4 bar pool units within the meander sections to avoid entrance and exit effects.

For the high-pass topographic grid containing the dune topography, dune geometries were characterized by performing a zero-crossing analysis on a manually-delineated trace drawn along the channel which captures a typical path along which dunes were most frequently observed throughout the experiment (Figure 5a). Although this approach does not capture all the dunes for any one topographic dataset, we found it to provide a consistent characterization of dune geometry across all our datasets. Zero-crossings along the elevation profile of the trace were used to identify local maxima and minima which defined the dune crests and troughs. Dune

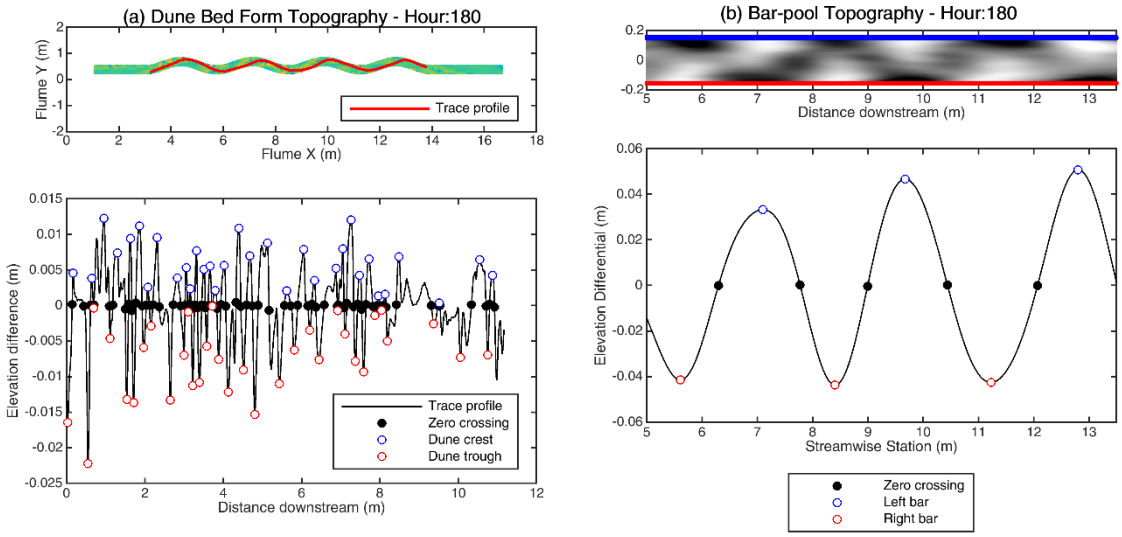

Figure 5 Example of zero-crossing analysis for the high-pass and low-pass gridded topographic datasets. (a) Results from the high-pass gridded data containing the dune topography at hour 180. (b) Results from the low pass gridded data containing bed form topography.

heights were defined by the elevation difference between a crest and downstream trough. Dune wavelengths were measured by the distance between two subsequent dune crests. Average values of the amplitudes and wavelengths of all dunes identified along the trace were used to characterize the dune morphology for each topographic dataset.

2.13 Bed Observations and Dune Spatial Tracking

Observations of the flume bed were made every 30 minutes throughout the last 16 hours of Run 1 and all of Run 2 to track the spatial extent of actively migrating dunes and any notable bed morphological changes such as exposed bars and depositional trends. These observations were recorded as hand-drawn sketches onto pre-printed worksheets with an outline of the flume walls, and grids of the local coordinate system. Dunes were only noted if visible transport was observed on the bed forms. If dunes became inactive relict features over multiple observation periods or if they were determined to be part of larger depositional trends, they were noted but not mapped as active dunes. Some subjectivity is inherent in these types of observations; however, in aggregate they provide significant insights into the spatial and temporal patterns that would otherwise be difficult to quantify. These sketches were later georeferenced and digitized using QGIS to create shapefiles representing the spatial and temporal locations of active dunes at Equilibrium 1 and throughout all of Run 2. MATLAB® processing was used to generate two visualizations from these sketches: 1) a space-time raster map tracking the fraction of each cross section occupied by dunes throughout the experiment, and 2) spatial probability plots that represent the fraction of time an area was observed with dunes based on the number of observations made during the determined time.

2.14 Bed Roughness Mapping

Direct or photographic measurement of the grain-size distributions of the entire flume bed was not possible due to the fine-grain bed sediments, so we characterize bed surface texture using a roughness proxy calculated from the ultra-high resolution DEMs. First, a DEM of grain-scale topography was created by applying a moving-average window across the original DEM and subtracting the mean windowed elevation from the raw elevations. The grain-scale DEM was then processed by a moving window standard deviation filter that calculated, for each pixel on the DEM within the moving window range, a standard deviation of the grain-scale elevations. This produced a map of standard deviations where larger standard deviations correspond to coarser sediments and increased void spaces on the surface. The DEMs used for this analysis had pixel resolutions of 0.083 mm and used a moving-average window size of 2 mm for the skin roughness extraction and a standard deviation window size of 4 mm.

To track the changes in roughness over time, the DEM of standard deviations for Equilibrium 1 was divided into two classes, a "rough" class which included the areas with standard deviations in the top 25^{th} percentile of standard deviations (> 0.11 mm) and a "fine" class which included standard deviations less than the 25^{th} top percentile (< 0.11 mm). We found that subdividing the data into more, smaller standard deviation bins was not useful as this tended to capture the inherent background "noise" of the DEM likely related to inherent uncertainties in the DEM generation process. The class limits characterized for the Equilibrium 1 DEM were then applied to the subsequent DEMs to track changes during the experiment relative to Equilibrium 1.

3 Results

3.1 Overview of Runs 1 and 2

Figure 6 provides results for the entire duration of Runs 1 and 2 of the experiment. During the beginning of Run 1, deep pools and shallow bars became readily identifiable by 11.3 hrs as the flume bed developed bar-pool morphology (Figure A2a and A3a). A non-uniform settling of the bed was observed during the first hours of the run due to the consolidation of previously unsaturated bed sediments, which contributed to a notable drop in bed slope from 0.0039 to 0.0026 between 0 and 17.3 hrs (Figure 6b), after which the bed appeared to have largely stabilized. In response to the settling of the bed, several large depositional features were observed forming along the length of the flume as sediment wedges formed in depressed elevation areas.

Sediment transport was not continuous throughout the flume initially, as reflected in the bed load transport rates which dropped from the initial rate of 23.6 g/min to 1.2 g/min by 17.3 hrs (Figure 6a). Sediment transport continuity was first observed through the exit section of the flume at 16.1 hrs and soon after bed load transport rates began to increase. The bed load transport during Run 1 peaked at 35.7 hrs at a rate of 21.0 g/m, with a sustained high average rate of 19.7 g/min between 30.7 to 38.8 hrs, before declining and stabilizing around 12.4 g/min during the last 16 hours of Run 1.

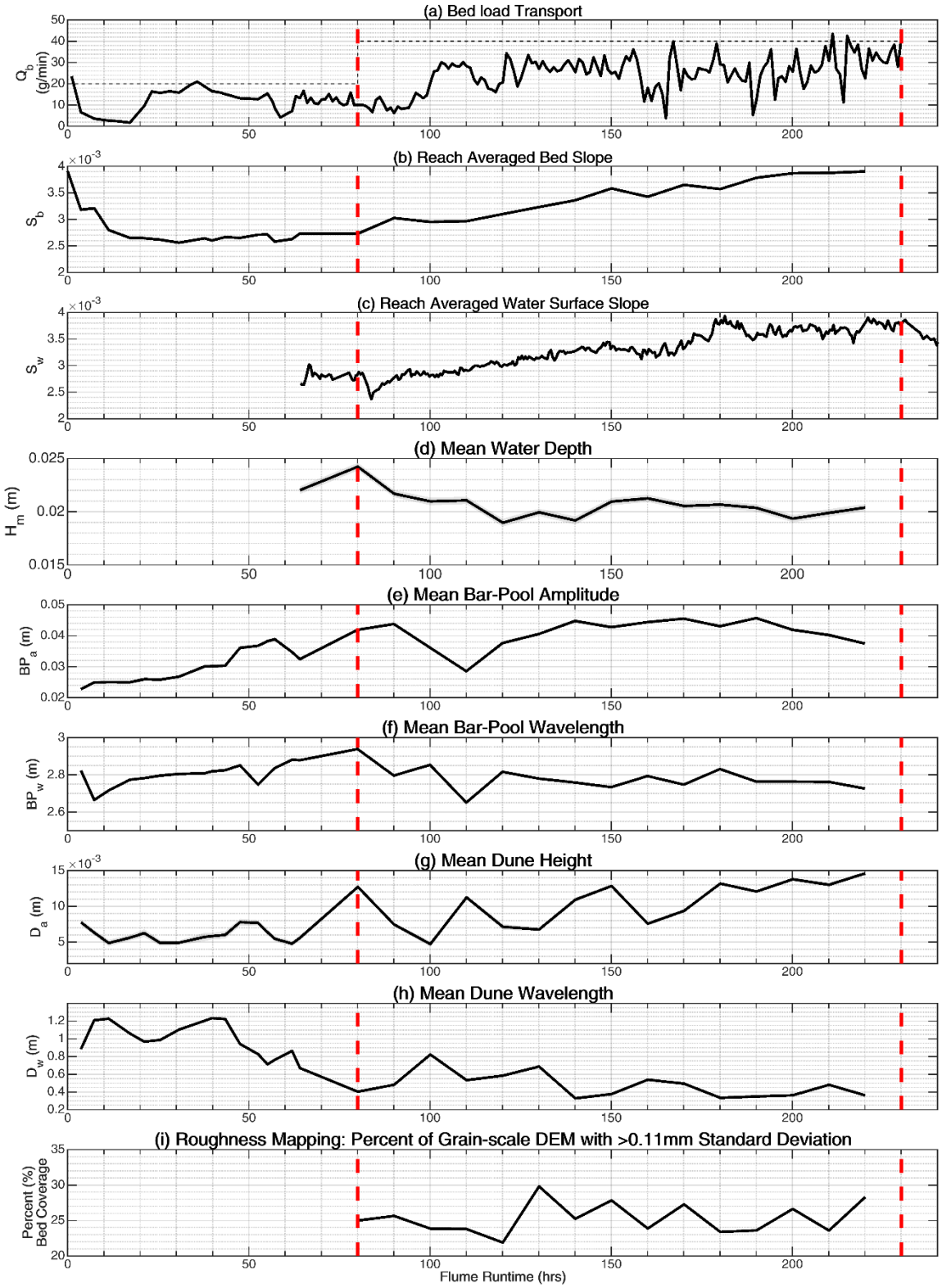

Figure 6 Results for the entire experiment of: (a) hourly averaged bed load transport, with horizontal dashed lines indicating the sediment feed rate, (b) reach-averaged bed slope, (c) reach-averaged water surface slope, (d) mean water depth, (e) mean bar-pool amplitude, (f) mean bar-pool wavelength, (g) mean dune height, (h) mean dune wavelength, and (i) percent coverage of rough facies type, as determined by the standard deviation roughness mapping procedure and defined by the top 25th percentile standard deviations from Equilibrium 1 roughness DEM. Vertical dashed lines indicate the end time of Runs 1 and 2.

The first dunes were noted at 14.3 hrs, after which dunes were only occasionally observed in isolated occurrences until the period between 33.7 hrs and 37.8 hrs, when multiple, more persistent, dunes were observed along the channel. Between 43.5 and 47.6 hrs, long "patches" of multiple dunes in succession were noted forming along the channel thalweg. For the remainder of Run 1, dune patches appeared with greater frequency and often extended and migrated downstream from their initial observed location. Dune patches were also observed to disappear and be smoothed over as sediments transported from upstream deposited on them. Direct recording of the spatial extent of dunes on the bed began during the final 16 hours of Run 1, from 64.1 hrs to 80.1 hrs. Run 1 was confirmed to have reached a quasi-equilibrium state at 80.1 hrs, as determined from the observation of a stable bed slope of 0.0027 and average water surface slope of 0.0028 during the last 16 hours of the Run 1. Bed load grain-size distributions were also found to be largely similar to the sediment supply (Figure 7b).

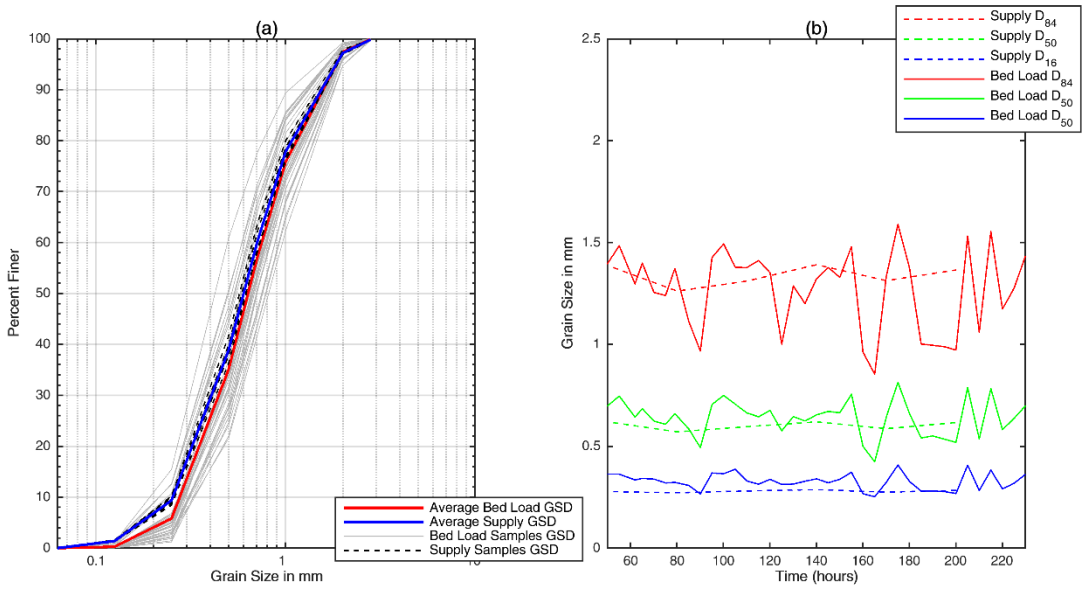

Figure 7 Comparison of sediment supply grain-size distribution metrics with the bed load samples. a) Grain-size distributions for sediment supply and bed load samples, with average grain-size distributions for both. b) Key grain-size metrics from the sediment supply and bed load samples over time.

When the sediment supply was doubled for Run 2, the bed load transport measured at the tailbox remained relatively stable for 10 hours before an increase was observed (Figure 6a). Dune bed forms were commonly observed throughout Run 2. The duration of Run 2 lasted 150 hours from 80.1 hrs to 230.1 hrs, until a new quasi-equilibrium condition was able to be confirmed. However, the magnitude of changes observed after 190.1 hrs decreased significantly, likely indicating that equilibrium conditions were achieved prior to 230.1 hrs. At Equilibrium 2, the average bed slope stabilized at 0.0039 between 200.1 hrs and 220.1 hrs. Although Run 2 was continued until 230.1 hrs, the SfM model generated for that time was found to contain systematic doming errors that could not be rectified and has been excluded from our topographic analysis (Figure 6b, d, e, f, g, h). Data for 220.1 hrs will be used to discuss Equilibrium 2 conditions, where appropriate. Water surface slope measurements largely stabilized after 190.1 hrs and averaged 0.0037 during the last 20 hrs of Run 2. The bed load transport rate during the last 20 hrs of Run 2 stabilized at 32.3 g/min and bed load sediment grain-size distributions matched well to the bulk sediment supply throughout Run 2, indicating that, on average, all grain-size fractions were generally mobile (Figure 7).

Although the bed load transport exiting the flume never fully matched the rate of sediment input, a morphological equilibrium was observed for both Equilibrium 1 and Equilibrium 2, where changes in the physical bed were largely stabilized (Figure 8). We suspect that the deficit in observed bed load transport likely stemmed from the initial bed being placed while damp, yet unsaturated, which would have had a greater initial porosity than a bed of bulk material that was fully pre-saturated with water. It is likely that the consolidation observed during the first hours of Run 1 continued after 17.1 hrs, albeit at a greatly reduced magnitude, due to filling/draining the bed and transport processes reworking the bed surface sediments. Our

observations of the dynamic equilibrium conditions indicated that the major physical adjustments were complete regardless of this transport deficit.

3.2 Bed Slope Adjustments

During Run 2, the reach-averaged bed slope increased by 44 percent from 0.0027 to 0.0039 from 80.1 hrs to the end at 220.1 hrs (Figure 6b, and Figure 8). As mean bed slopes increased throughout Run 2, the mean depth decreased from 0.024 m at 80.1 hrs to 0.02 m at 220.1 hrs (Figure 6d). The depth change occurred rapidly at first, with a 16% decrease occurring between 80.1 hrs and 120.1 hrs, after which after depths fluctuated between 0.019 m and 0.021 m and ended at 0.020 m at 220.1 hrs, a 16.7% decrease from Equilibrium 1 conditions. Width-to-depth ratios increased from 14.2 at 80.1 hrs to 16.9 at 220.1 hrs.

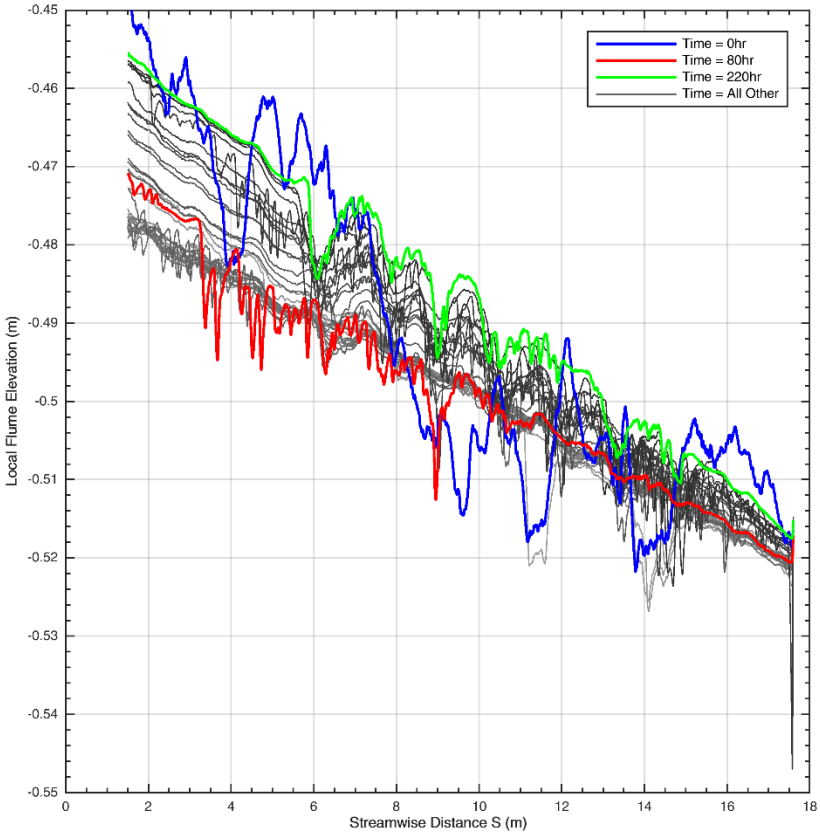

Figure 8 Mean bed profiles for Runs 1 and 2. Initial, Equilibrium 1 and Equilibrium 2 average bed profiles are identified by color, other profiles are plotted with a gradient of grey, from light to dark, representing times from the start to the end of the experiment (0 hrs – 220.1 hrs).

3.3 Bar-Pool Bed Form Adjustments

The mean bar-pool wavelength remained relatively consistent throughout the entire experiment, averaging 2.79 m with some fluctuations that varied above and below the mean by 5% and 5.3%, respectively (Figure 6f). There was an initial decline in the bar-pool wavelengths between hours 3.7 and 17.2, likely due to how the developing bar-pool morphology and bed settling was interpreted by the zero-crossing analysis. The largest decrease in mean bar-pool wavelength, down 5.3% from the mean to 2.65 m, occurred at 110 hrs, 30 hours after the sediment supply was doubled. The largest average bar-pool wavelength of 2.94 m occurred at 80.1 hrs, at Equilibrium 1.

Bar amplitudes generally increased during Run 1 from 0.023 m at 3.6 hrs to 0.042 m at 80.1 hrs, indicating the developing bar-pool morphology from the initially plane bed (Figure 6e). After doubling the sediment supply at the start of Run 2, there was a slight increase in bar amplitude to 0.044 m at 90.1 hrs followed by a persistent decrease for 20 hours to a minimum of 0.029 m at 110 hrs, a 31% decrease from the amplitude at Equilibrium 1. Subsequently, the mean bar-pool amplitude increased over the next 30 hours to 0.045 m at 140.1 hrs, 7.1 percent higher than the amplitude at Equilibrium 1. After 140.1 hrs, the mean bar-pool amplitude remained relatively consistent for the remainder of Run 2. No substantial decreases in mean bar-pool amplitude was observed after the low at 110.1 hrs. At the end of Run 2, the mean bar amplitude was 0.037 m, 12% lower than at 80.1hrs, and the average between 140.1 hrs and 220.1 hrs was 0.042 m.

3.4 Dune Bed Form Adjustments

Migrating dunes were a common observation during the experiment after 30.7 hrs into Run 1. These bed forms were commonly arranged in groups of multiple dunes but sometimes

occurred as single dunes that appeared, migrated, and disappeared periodically throughout the experiment. Typically, dunes first appeared along the thalweg along the outer bank, in the pool where secondary flow patterns would be expected. The dunes usually began as small, hardly distinguishable, rough patches of sediments or perturbations in the bed that, over time, grew larger as they migrated along the bed. Often times, additional dunes formed downstream of the initial dune creating trains of dunes that migrated down the channel following the thalweg, alternating from one side of the channel to the other, slightly out of phase with the channel planform (Figure 11c). Dune crests were typically oriented perpendicular to the flow pattern, sometimes skewed in relation to the higher velocities nearer to the center of the channel. At various times the dune patches expanded and covered the entire bed, covering both the bars and the pools.

The development of the dunes can be identified in Figure 6g and Figure 6h from the increase in dune heights and decrease in dune wavelengths up until the end of Run 1 at 80.1 hrs. As the channel approached Equilibrium 1, the mean dune height was observed to increase from 0.005 m to 0.013 m between 61.9 hrs and 80.1 hrs (Figure 6g). The increase in dune height during this time corresponded with a decrease in the average wavelength between dunes, from 0.86 m down to 0.40 m. Reported dune heights of less than 0.005 m were generally indicative of a lack of dune presence along the bed as can be seen from the lack of dunes in the high-pass and detrended topography at 61.9 hrs (Figures A1a, A3a). Similarly, relatively long dune wavelengths, such as 0.86 m at 61.9 hrs, were also indicative of a bed generally devoid of dunes. During the final 16 hours of Run 1, a well-developed set of dunes had formed on the bed.

During Run 2, mean dune heights decreased from 0.013 m to 0.005 m between 80 hrs and 100 hrs while the wavelength increased from 0.4 m to 0.82 m. These reported measurements

indicate that the dunes had a decreased presence over the first 20-hours after doubling the sediment supply. This observation was further confirmed from the visualizations of the dune spatial tracking sketches provided in Figure 9 and Figure 10. For the remainder of Run 2, between 100.1 hrs and 220.1 hrs, the dune heights trended higher, while the dune wavelengths trended lower. The zero-crossing analysis of our topographic datasets indicated oscillations between periods of time with high and low average dune heights and short and long dune wavelengths after 100 hrs until the end of Run 2. During this time, the low dune heights in this oscillating trend never revisited the low attained at 100 hrs, while the high points in the trend tended to increase, but never significantly higher than at Equilibrium 1. The highest reported average dune height was 0.015 m at 220.1 hrs, a 15% increase from Equilibrium 1, and were within 7.6% (0.014 m) when averaged between 200.1 hrs to 220.1 hrs. Dune wavelengths at 220.1 hrs were 0.36 m, 10% lower than Equilibrium 1, and relatively unchanged (0.4 m) when averaged between 200.1 hrs and 220.1 hrs.

3.5 Spatial and Temporal Dune Observations

Figure 9 summarizes the spatial and temporal patterns of dunes for the last 16 hours of Run 1 at 64.1 hrs until 20 hours after the end of Run 2 at 250.1 hrs. In the figure, temporal variability in the presence of dunes is indicated by horizontal banding of color that changes as dunes were observed to appear and disappear. Migrating dune patches can be identified by a diagonal banding pattern along the upstream or downstream edge of the colored bands, while locations of persistent dune patches are indicated by consistent bands of color down the plot in the vertical direction. The color represents the fraction of the bed width covered in dunes, where yellow intensities indicate that the full width of the channel was covered by dunes and cooler

intensities represent only partial coverage, such as when dune patches were in long trains along the thalweg only.

Dunes were persistently observed downstream of the bend apices on the outside of the bends, just downstream of where the high-velocity flow cores were deflected by the channel wall. For example, between the middle and end of Meander 1 (M1) at approximately 6 m down the channel, dunes were nearly always observed. The dune observations shown in Figure 9 confirm several observations discussed in section 3.4, including the development of large migrating patches of dunes at Equilibrium 1 as identified from the large bands of color that

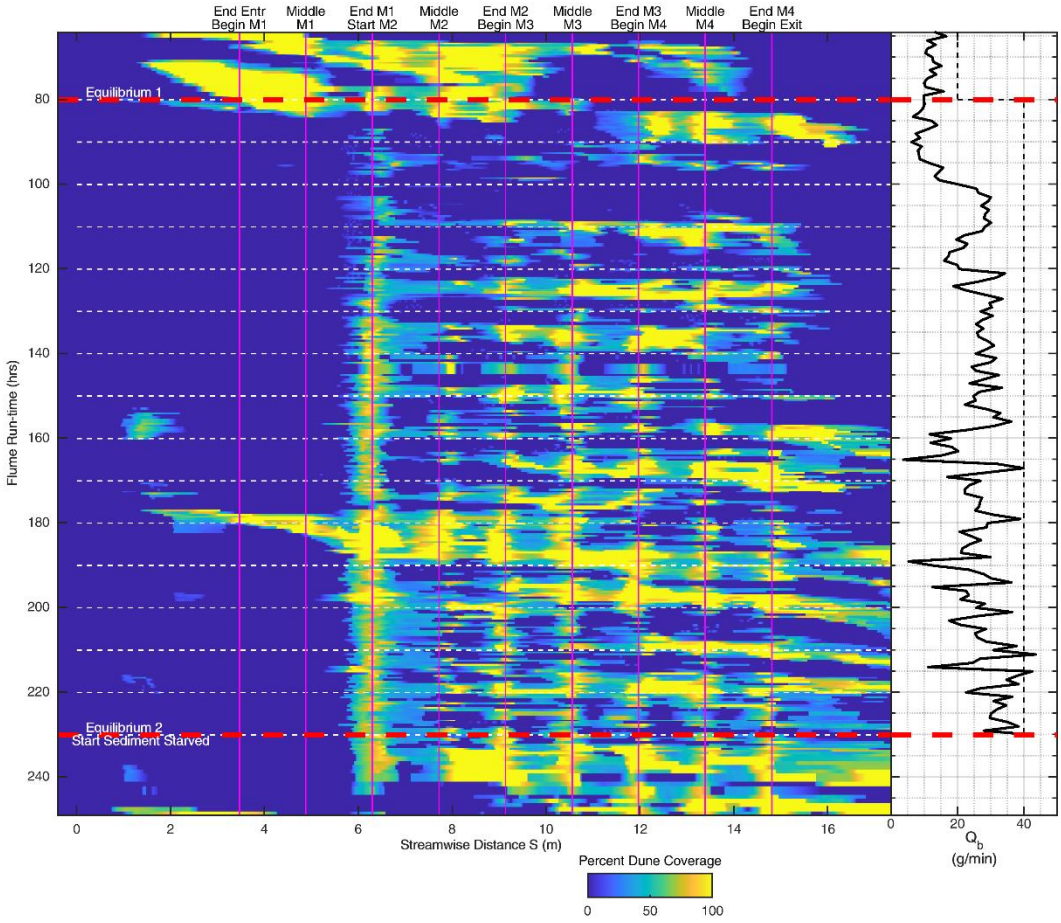

Figure 9 Temporal raster plot of dune coverage on the flume bed alongside bed load transport rate. Color gradient represents the percent of the cross section covered in dune patches. Red lines denote the Equilibrium 1 and Equilibrium 2 conditions that bracket Run 2.

appeared and migrated downstream between 64.1 hrs and 80 hrs. Additionally, the significant decrease in dune presence in the beginning of Run 2, between 80 hrs until just before 110 hrs, can be seen from the low intensity banding during this time period. This trend started with a significant smoothing of dunes in the upper 12 m of the flume during the first 10 hrs after supply was doubled, followed by nearly 20 hours of very few dunes on the bed until just before 110.1 hrs. After this time, dunes began to redevelop, and continued to develop, migrate and disappear throughout the remainder of the Run 2 as can be identified from the horizontal color banding during this time. After Run 2, the flume was run for 20 additional hours in a sediment-starved condition, which appeared to have little impact on the occurrence or spatial distribution of dunes. This served to help confirm that the dune formation observed during the experiment was not likely caused by the methods used to supply sediment to the flume, in small batches every 5 minutes.

Some of the variability in the measured average bed load transport rates was observed to correspond with the spatial distribution of dune bed forms. The first significant increase in bed load transport during Run 2 did not begin until a significant decrease in dune coverage occurred at 100.1 hrs (Figure 9). Additionally, periods of low bed load transport also correlated with times in which dune bed forms covered at least a portion of the downstream portion of the exit section. On multiple occasions this was observed to cause a pocket to form against the sediment weir where turbulent eddies formed. Once deposition in the pocket smoothed the surface, bed load transport rates increased.

3.6 Spatial Probability of Dunes

The spatial probability plots shown in Figure 10 provide a more visual perspective of many of the trends observed with the dune bed forms that have been discussed in Sections 3.3 and 3.4.

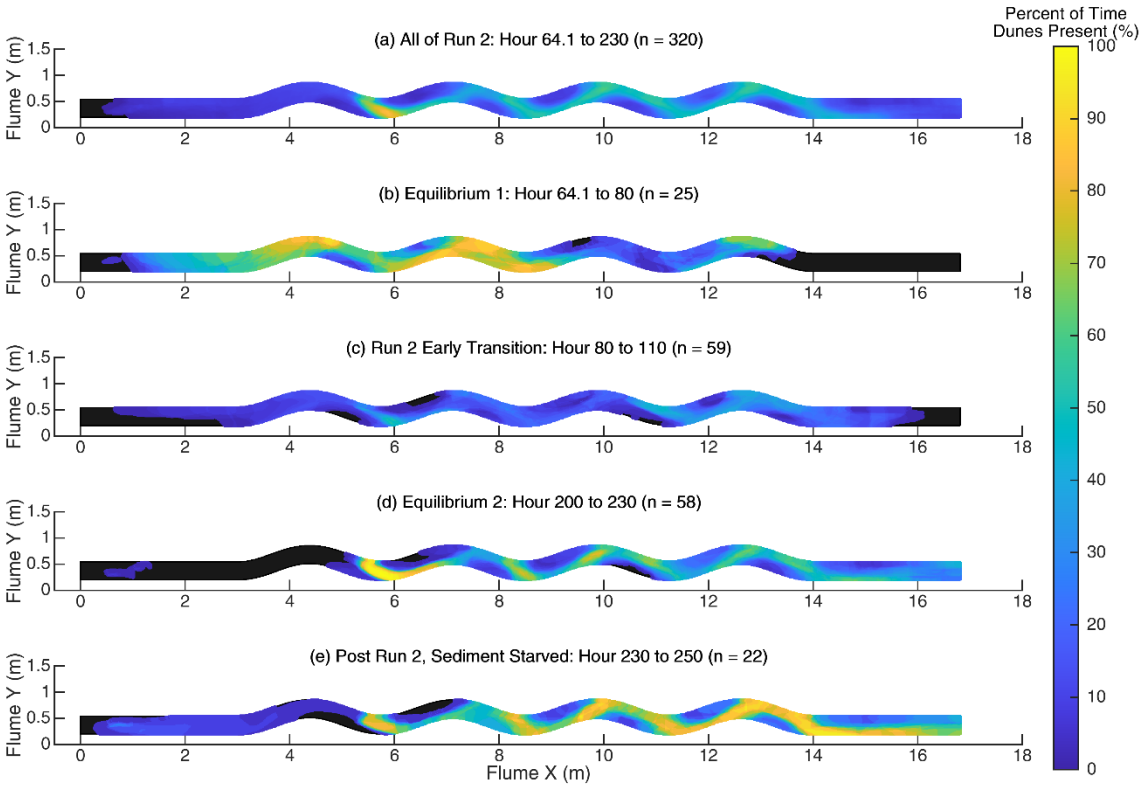

Figure 10 Spatial probability plots from observations of the bed for specific time periods during the experiment, including: (a) the entire duration of Run 1, (b) last segment of Run 1 during which Equilibrium 1 was confirmed, (c) first 30 hours of Run 2, early in the transition to the increased sediment supply, (d) last 30 hours of Run 2 where Equilibrium 2 is established, and (e) 20 hours after Run 2, which was run in a sediment-starved condition.

Throughout the last 16 hours of Run 1 and Run 2, dunes were most likely observed along the thalweg, alternating from pool to pool, with observations of dunes covering the entire width of the channel being much less frequent (Figure 10a). The location where dunes were observed most frequently can be seen along the second half of Meander 1, where they were noted in greater than 90% of all flume observations. During Equilibrium 1, it can be seen that dunes occurred more frequently in the upstream portions of the flume, they often covered large portions of these areas more than 50% of the time, and they were never observed extending into the exit section (Figure 10b). Dunes were also observed during Equilibrium 1 as far upstream as the entrance section, which was not observed nearly as frequently early during Run 2 (Figure 10c) or Equilibrium 2 (Figure 10d). During Run 2, it was significantly less probable to observe dunes

over large portions of the bed during the first 20 hours after the sediment supply was doubled (Figure 10c), as compared to the other time periods shown (Figure 10b, d, e). There were only select locations along the flume during this first 20 hours where dunes were observed 50% or more of the time, while in most parts of the bed dunes were observed 30% or less of the time. During the last 30 hours of Run 2, selected to represent Equilibrium 2, dunes were much more likely to be observed along the thalweg of the channel (Figure 10d). During this period of the experiment dunes were primarily observed extending from the middle of Meander 1, downstream through the end of the exit section. During the sediment-starved condition after Run 2, the spatial observance of dunes was very similar to Equilibrium 2, with the exception that dunes were seen in the entrance section during approximately 10-20% of observations.

3.7 Sediment Sorting Adjustments

Patterns of sediment sorting are presented in Figure 11a-e for Equilibrium 1 and Equilibrium 2. Both the hand drawn facies maps (Figure 11a, d) and the standard deviation roughness mapping (Figure 11b, e) indicated similar sorting patterns on the flume bed for each respective equilibrium. Generally, sediment sorting patterns at Equilibriums 1 and 2 and indicated the development of coarse patches in the pools, along the thalweg, where flows were convergent with the wall. Patches of fine sediments were observed on the bar tops downstream of bend apices, in areas sheltered from the higher velocity flows. Sorting patterns were also observed to vary spatially and temporally in conjunction to the presence of dunes, and course and fine patches were often observed followed the course of the thalweg at cross-overs when dunes were present (Figure 11a-f). Coarse patches were observed in dune troughs and fine patches were observed on the dune crests which changed rapidly as dunes migrated through the channel.

The hand-drawn facies mapping indicated a fining of the bed between Equilibriums 1 and 2. Of the area recorded on the facies maps, course patches decreased from 14.5% to 4%, medium patches increased from 61.5% to 67.1%, and fine patches increased from 24.5% to 28.9% (Figure 11a, d). Grain-size samples of the patches indicate that the coarse patches got coarser between Equilibrium 1 and 2, with the d_{50} increasing from 0.69 mm to 0.95 mm. The medium patches were found to remain essentially unchanged, changing only from 0.51 mm to 0.52 mm between equilibriums, and the fine patches got slightly finer, decreasing from 0.38 mm to 0.35 mm, respectively. Area-weighted surface grain-size d_{50} for the entire mapped area decreased slightly between Equilibrium 1 and 2, from 0.51 mm to 0.49 mm. Simply summarized, the areal extent of fine and medium facies increased and the extent of the coarse facies decreased during Run 2; fine patches became slightly finer, coarse areas became coarser, and medium patches remained relatively the same.

Temporal mapping of the roughness proxy described in Section 2.14 from the grain-scale DEMs generally corroborates the response of the bed shown in the facies mapping (Figure 11b, e). The roughness mapping used a slightly different metric, based on solely on surface texture rather than texture and grain-size, and detected a very slight decrease in the rough areas of the bed with standard deviations greater than 0.11 mm between 80.1hrs and 230.1 hrs. The percent coverage by areas classified as rough was 25 percent at 80.1 hrs and fluctuated between a low of 21.9 percent at 120 hrs and a high of 29.8 percent at 130.1 hrs, with no discernable trend throughout Run 2. Although a transient minimum between equilibrium conditions was observed at 120.1 hrs, it is not known if a 3.1% decrease in roughness is within the threshold of detection for our roughness mapping procedure and should be considered with caution (Figure 6i). Rather, we consider results of the roughness mapping as largely corroborating the sorting pattern and

fining trends identified on the hand-drawn facies maps during Run 2, however small the overall effect on the bed grain-sizes. Therefore, we believe the impact on bed load transport was likely not significant.

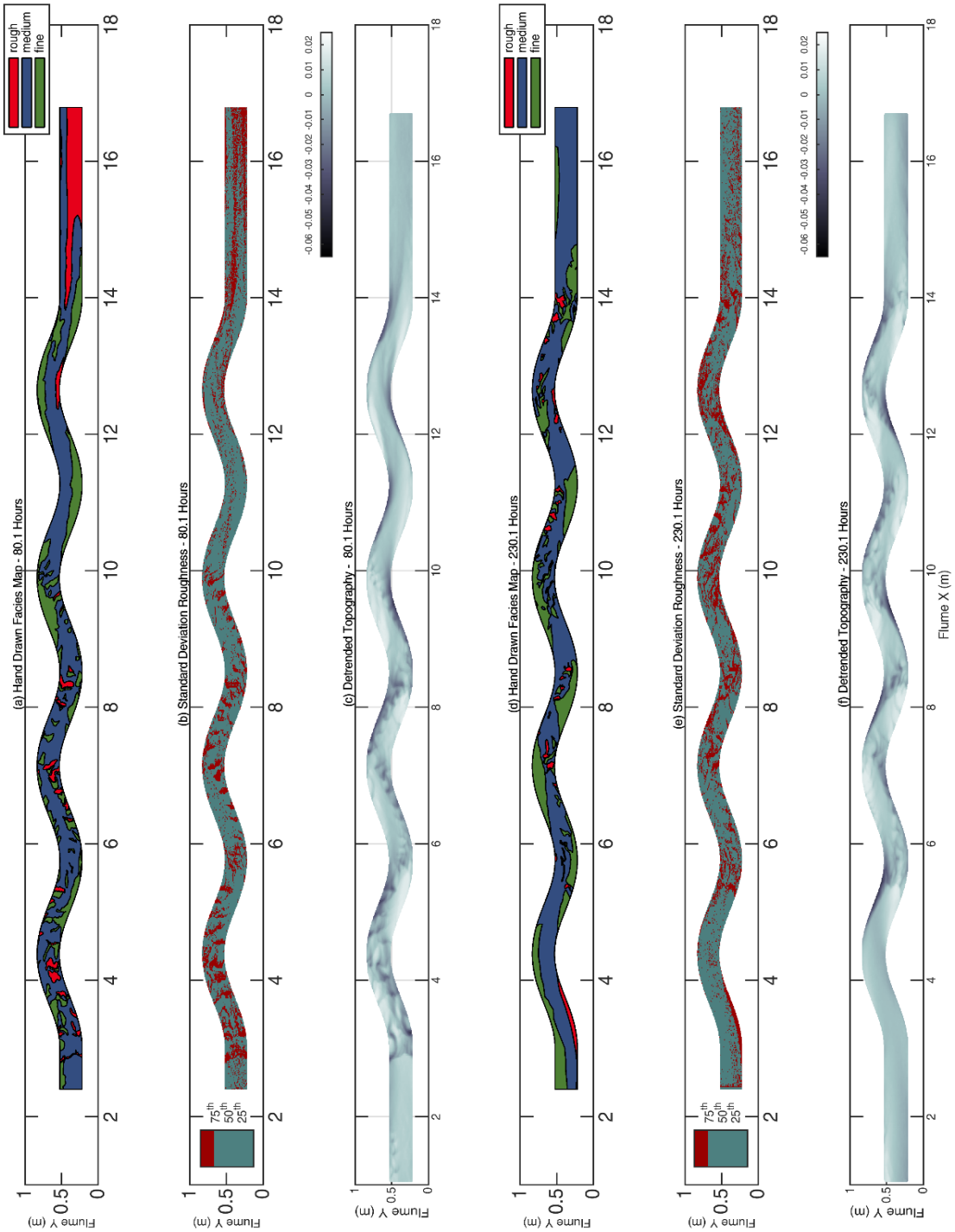

Figure 11 Sorting patterns from Equilibrium 1 and Equilibrium 2. (a, d) Hand drawn facies map at 80.1 hrs and 230.1 hrs, respectively. (b, e) Standard deviation roughness maps at 80.1 hrs and 230.1 hrs, respectively. (d, f) Detrended topography at 80.1 hrs and 230.1 hrs, respectively.

4 Discussion

4.1 Temporal Progression of Channel Response to Increased Sediment Supply

Following the ideas of Buffington (2012), we expect the channel response to increased sediment supply to progress from small scales (grain size) to larger ones (bar morphology, slope), in order of increasing magnitude of geomorphic work required. We focus on the following reported measurements to illustrate the temporal progression of the channel response: 1) the grain-scale roughness proxy (Figure 6i), 2) cross-sectional scale mean dune amplitude (Figure 6g), 3) meander-scale mean bar-pool amplitude (Figure 6e), 4) reach-scale average bed slope (Figure 6b), as well as the bed load transport measurements (Figure 6a).

Although grain-scale roughness was difficult to quantify in our experiment, previous research indicates that the fining of surface sediments is a plausible first response if sediment supply overwhelms capacity (Eaton & Church, 2009). Although our channel may have exhibited temporary and local areas of surface fining, we did not detect those in our measurements and the bed roughness proxy was largely unchanged from Run 1 to Run 2 (Figure 6i). This is not necessarily surprising, because a) the range of sizes in the bulk grain size distribution was somewhat narrow (Figure 3) and b) the fully-mobile conditions of Run 1 resulted in a bed that was generally unarmored (e.g., (Venditti et al., 2017)). The grain-scale response (spatial scale ~ 0.00062 m), therefore, was not a major component of the overall channel response to the sediment supply increase.

At the cross-section scale, changes occurred to the smaller-scale dune bed forms (spatial scale ~ 0.4 m). The development of dunes during Equilibrium 1 agrees with bed-state phase diagrams, which indicate our experimental hydraulic conditions were in the range favorable for

dune development (Southard & Boguchwal, 1990; Carling, 1999; Kleinhans, 2005). Furthermore, the high sediment supply during Runs 1 and 2 also provided conditions favorable for the development of scaled gravel dunes (Pitlick, 1992; Venditti et al., 2017). The dunes exhibited a maximum response at 100.1 hrs when they became largely absent from the flume (Figure 9), and the dunes that did remain had decreased average height (Figure 6g). This likely reduced overall form drag and increased the overall sediment transport capacity in the channel temporarily, although the dunes redeveloped shortly afterward and their height progressively increased throughout the rest of the experiment.

At the meander-scale (length scale ~2.79 m), the bar-pool morphology responded to the sediment supply increase with a temporary decrease in bar amplitude, which was most pronounced at 110.1 hrs (Figure 6e). Experiments in variable-width straight channels have shown that bar-pool relief can decline in response to supply increases (Morgan, 2018), and field studies of dam removal have observed temporary pool-filling due to sediment supply increases (East et al., 2015). In our experiment, the reduction in bar amplitude should have decreased overall form drag and increased transport capacity, and as the bar height subsequently increased again slope adjustments (discussed below) likely maintained the increased transport capacity.

At the reach-scale, the bed slope increased 44 percent over the course of Run 2, but at a much slower rate than the smaller-scale responses. While the dunes and bar morphology were temporarily adjusting, the bed slope response was essentially paused, as seen by the plateau in the increasing average bed slope between 90.1 hrs and 110.1 hrs (Figure 6b). During this pause in the bed slope response, sediment transport continued to increase, indicating that the response of the dunes disappearing and subsequent decrease in topographic relief from the bar-pool filling was likely temporarily decreasing bed form resistance resulting in increased transport capacity.

Once the smaller-scale responses were observed to reach their maximum effect, slope became the dominant response for the remainder of the run.

The reductions in dune and bar-pool amplitude were found to be largely transient, in that soon after their maximum response, as slope continued to increase, their amplitudes began to adjust back toward their Equilibrium 1 state. Throughout the remainder of Run 2, fluctuations in the bar-pool amplitude and dune height indicate that dynamic interactions between the channel response mechanisms were constantly evolving. By the establishment of Equilibrium 2, the dunes and bar-pool morphology were similar as in Equilibrium 1, which supports the idea that slope increase was the dominant long-term response.

4.2 Meandering Channel Response as System Wide Resistance Optimization

To better understand the response of our channel, we considered its total system resistance as described by from Eaton et al. (2004):

$$fsys = f' + f'' + f'''$$ (1)

where the system roughness $fsys$ is defined as:

$$fsys = \frac{8gRS_v}{u^2}$$ (3)

where S_v is the valley slope, g is gravitational acceleration, R is the hydraulic radius, and u is the mean channel velocity. As such, the system is understood to have a quantifiable total resistance imposed on the system by the dominant independent variables of discharge, sediment supply and valley slope. Eaton et al. (2004) hypothesized that this total system resistance is maximized when the system is at equilibrium. The components of total system resistance can be derived using the Darcy-Weisbach friction factor *f* using the bed slope *S*:

$$f = \frac{8gRS}{u^2} \tag{4}$$

to quantify the total within-channel resistance to flow. Grain-scale resistance can be approximated by the methods of Millar (1999):

$$f' = \left[2.03 \log\left(\frac{12.2Y}{k_s'}\right)\right]^2 \tag{5}$$

where Y is the flow depth and k_s' is the roughness height, assumed equal to the surface d_{50} (Nikuradse, 1933). The within-channel resistance due to dunes, bed forms, and other types of in-channel features f'' is the difference between the grain-scale resistance to flow and the total within-channel resistance to flow:

$$f'' = f - f' \tag{6}$$

The reach-scale form resistance due to sinuosity f''' is then equal to the remainder of the total system resistance after subtracting the within-channel resistance:

$$f''' = fsys - f \tag{7}$$

In our experiment, doubling the sediment supply in Run 2 reduced the equilibrium value of total system resistance $fsys$ for the meandering channel system, as total system resistance would have to decrease in order to increase transport capacity. This would need to be accomplished through reductions in f', f'', or f'''.

Using Equations (1) and (3)-(7), the impact of a sediment supply increase on total system resistance during this experiment may be calculated for both Equilibrium 1 and Equilibrium 2. Using the prescribed flow rate, reach-averaged depth, reach-averaged bed slope, area-weighted d_{50}, and assuming a rectangular cross section, we estimated the total system resistance and each component of resistance for our experiment (Table 2). In these calculations, the valley slope was

calculated as the slope of a straight line between the upstream and downstream weirs in the flume. These calculations show that $fsys$ was reduced from 0.13 to 0.088 between Equilibrium 1 and Equilibrium 2. Total within-channel resistance decreased slightly but remained largely the same (0.76 to 0.75), which is consistent with the observed lack of significant surface-sorting changes and largely unchanged bed form conditions between the two equilibria. Once the grain-scale resistance component is extracted, the model highlights the relatively consistent influence of both grain-scale changes f' (0.32 to 0.33) and bed form resistance f'' (0.44 to 0.42) at both equilibrium conditions. Most importantly, the model correctly highlights that the majority of decrease in total system resistance came from the reduction in the form resistance due to sinuosity f''' (0.54 to 0.14), via the dominant response of a slope increase. In our flume experiment the sinuosity was fixed, so the effects of any increase in slope would ultimately decrease the total system resistance (Equation (3) and the relative importance of reach-scale resistance due to sinuosity, Equation (7)). Had our channel walls not been fixed, we might expect that our channel would have responded in other ways, such as channel straightening, avulsions, or cutoffs (Braudrick, 2013).

Table 2 Calculations of total system resistance at Equilibrium 1 and Equilibrium 2

Time (hrs)	Flow Rate $\left(m^3/s\right)$	Width (m)	Mean Depth (m)	Area (m^3)	Wetted Perimeter (m)	Hydraulic Radius (m)	Bed Slope (m/m)	Mean Velocity ($^m/_s$)	Valley Slope (m/m)	D_{50} (m)	***fsys***	***f***	***f'''***	***f''***	***f'***
80.1	0.002	0.344	0.024	0.008	0.39	0.021	0.0027	0.24	0.004618	0.00051	**0.130**	**0.076**	**0.054**	**0.044**	**0.032**
220.1	0.002	0.344	0.021	0.007	0.39	0.019	0.0039	0.28	0.004618	0.00049	**0.088**	**0.075**	**0.014**	**0.042**	**0.033**

4.3 Conceptual Model of Channel Response and Response Potential

The idea of channel response as a modification to a total system resistance serves as a convenient conceptual model to seek answers to some of the more complex and intriguing interactions observed during the response of our meandering channel to a doubling in sediment supply. For this purpose, we break down the bed form resistance f'' into f_d'' and f_{bp}'', representing the portion of bed form resistance attributable to the dunes and the bar-pool relief, respectively, such that:

$$f'' = f_d'' + f_{bp}'' \tag{8}$$

Substituting Equation (8) into Equation (1), and arranging the right hand side in order of increasing spatial scale we have:

$$fsys = f' + f_d'' + f_{bp}'' + f''' \tag{9}$$

which now includes all of the observed degrees of freedom that our fixed-wall experimental channel had to respond to a sediment supply increase.

As discussed previously, the observations from this experiment indicate that multiple scales of response were occurring simultaneously during the transition to Equilibrium 2, according to a timescale in proportion with the geomorphic work required. It seems reasonable to assume that each component of resistance in Equation (9) for the system has a maximum magnitude of response possible. For example, surface grain-size resistance f' adjustments would be impossible in a channel with a uniform sediment size, while bed form resistances f_d'' and f_{bp}'' would be limited to a scale where the bed forms are completely suppressed. These maximum response potentials are likely different and unique for each alluvial system, but the

cumulative effect must be able to provide a system-wide reduction in resistance such that the channel is able to fully adjust any new imposed condition.

We therefore propose a conceptual model for the response of an alluvial fixed-wall meandering gravel-bed system to altered sediment supply (Figure 12). The model describes channel responses across spatial and temporal scales, with particular attention to scale-dependent response potential and implicit constraints that may explain the channel response in our experiment. Using this model, we propose that our experimental system had a low response potential for grain-scale resistance change f', likely due to the lack of armoring of the bed

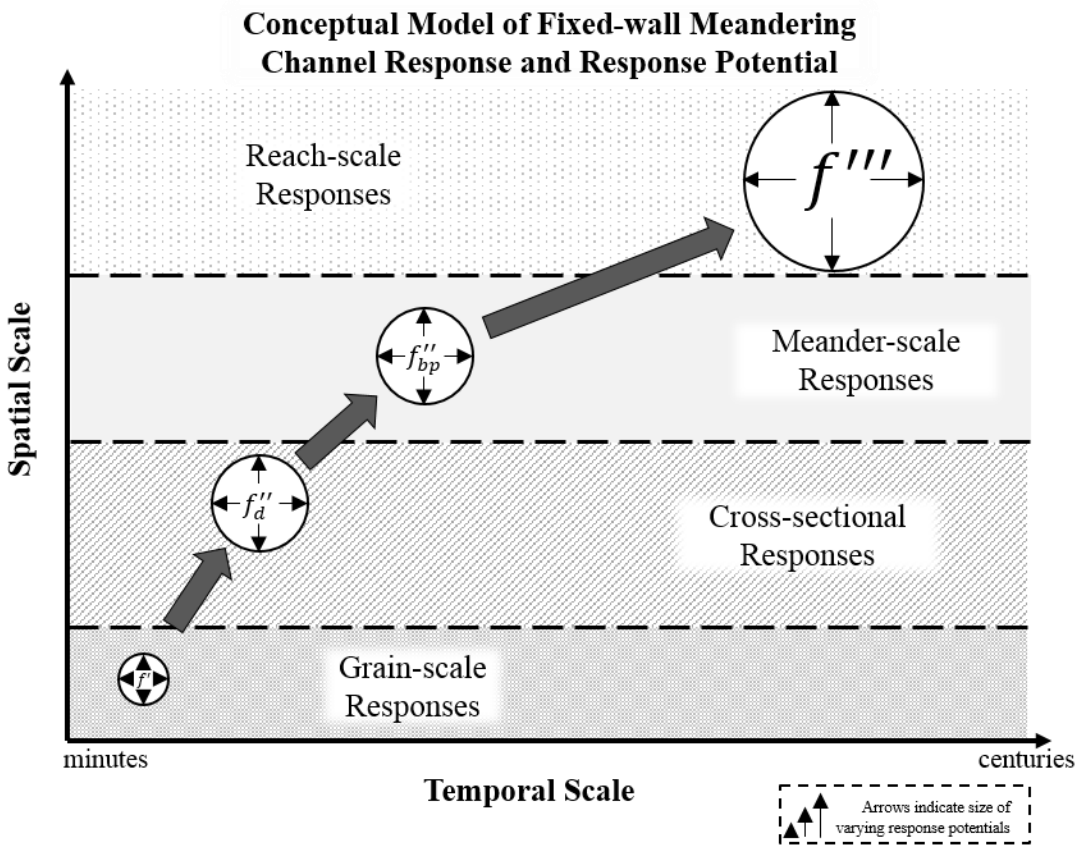

Figure 12 Conceptual model of fixed-wall meandering channel response. The magnitude of response potentials, indicated by arrow and circle sizes, have been idealized for the current flume experiment but are not to scale. f' represents resistance response potential for grain-scale adjustments, f_d'' represents resistance response potential for dune bed forms, f_{bp}'' represents resistance response potential for the bar-pool morphology, and f''' represents the response potential for system resistance due to sinuosity. The large arrow indicates the temporal progression of response in order of geomorphic work required.

sediments observed at Equilibrium 1 (Eaton & Church, 2009). This would explain why we saw little detectable response in the surface sorting and negligible contribution to the decrease of total system resistance $fsys$; that is, for our system f' is relatively fixed. The dunes present at equilibrium 1 had a higher response potential such that dune bed form resistance f_d'' could decrease more than f'. This matched well with our observation of a full suppression of dunes that reached its maximum response at 100.1 hrs.

If the total system resistance to the new sediment supply in Run 2 remained too large even after the dunes were largely eliminated, it could continue to adjust by further changing the larger-scale bar-pool morphology f_{bp}''. After the bar-pools were observed to achieve their lowest amplitude at 110.1 hrs, the only response with any potential left was a reach-scale slope increase that decreased f'''. Our observations confirm that this is what occurred for the remaining duration of Run 2. The unchanging slope between 90.1 hrs and 110.1 hrs can be interpreted using this model as an interaction between varying time and spatial scales of responses, where the smaller-scale responses with sufficiently large response potentials were occurring faster than the slower reach-scale adjustments, reducing the system resistance enough temporarily to increase transport capacity without requiring additional slope increases. Once the system had exhausted the full potential of these smaller scale responses, the slope continued to increase.

It is interesting to note that the two transitory responses, in the dunes and bar-pool morphology, largely returned to their original conditions after the shift to Equilibrium 2 was complete. This observation could indicate that at a long-enough time scale the slope increase alone provided a sufficient reduction in total system resistance to fully accommodate the sediment supply. This raises additional questions as to what influences the persistence of any one

scale of response in a meandering channel to a change in sediment supply. Perhaps at long time scales, the bar-pool morphology of our fixed-wall meandering channel is not influenced by sediment supply. Similar observations have been observed in the field and laboratory studies with variable width channels, where riffle-pool morphology was largely forced by channel planform (Brew et al., 2015). Similarly, gravel dunes may be more driven by hydraulic forces and a threshold of available sediment supply than a specific sediment supply. If true, so long as the new long-term equilibrium maintained the hydraulic and sediment supply conditions for gravel dunes to form, they could reestablish without increasing the system resistance too much. More research is needed to fully understand the transient nature of these responses.

4.4 Reconciling Previous Research on Meandering Channels

If we consider the response of a meandering channel to changes in sediment supply in terms of our conceptual model (Figure 12) we can more easily understand the wide range of results that have been reported in previous research and see that they may not be as contradictory as they appear. Similar to our experiment, Braudrick (2013) reported a slope increase and bed fining as the dominant responses of a meandering fixed-wall channel to a doubling in sediment supply. For his experimental system, if the potential for grain-scale resistance changes were low compared to the large change in sediment supply, and any bar-pool response is largely transient due to the forcing of channel planform, it follows that the only response with enough potential to accommodate their supply change would have also been an increase in bed slope. Interestingly, Braudrick (2013) noted dunes present on the fine facies of the bed at the start of his experiment but did not report any subsequent observations regarding them, so we do not know to what extent dunes may have influenced the response of the channel, even during the transition.

Erwin (2013) reported that in her experiment, the field-scale meandering flume accommodated a 5-fold increase in sediment supply via shoaling of pool and a lateral expansion of the bar. She concluded that the increase in sediment supply likely far exceeded the ability of textural changes to accommodate, which would imply that grain-scale response potential was low for her system. Additionally, the cobble riffles in the flume may have served as a hydraulic control, potentially fixing the reach-scale resistance due to sinuosity so that the only response readily available to the system was through cross-sectional scale changes, as she observed. Alternately, it was noted in Erwin (2013) that the transport though the system at the end of the high sediment run had not fully matched the 5-fold sediment supply increase. It is possible that due to the long time-scale required for a slope response in the flume, the experimental duration primarily captured the smaller time-scale responses. With a longer duration, a reach-scale slope-change may have eventually occurred.

Eaton and Church's (2009) observation that a doubling of sediment supply could be accommodated by fining the bed without significant slope change can be understood if we consider the differences in grain-scale response potential as compared to our experiment. In their experiments, they observed various degrees of armoring ratios, the ratio of the d_{50} of the surface to the subsurface material, that decreased as the imposed sediment supply increased. They observed that in flume runs where the armor ratio neared unity that the surface had no capacity to fine, and aggradation occurred. Eaton and Church (2009) went further to show on a theoretical basis that up to a 4-fold increase in sediment supply could be accommodated though a fining of the surface armor layer using Parker's (1990) fractional sediment transport relation. These observations imply that their alluvial system had a much higher potential for grain-scale resistance response than ours did, such that many of their experimental channels were able to

fully adjust to different imposed sediment supply conditions without much progression of the larger-scale responses.

4.5 Implications for River Management and Restoration

An improved understanding of the temporal and spatial progression of channel response should prove to be beneficial to river managers, engineers, ecologists, and those seeking to mitigate the impacts of sediment disturbance due to natural events or anthropogenic activity. Human activities such as dam construction and gravel mining operations often alter the natural sediment supply delivered downstream, (e.g., Williams & Wolman, 1984; Kondolf & Matthews, 1991), and have been observed to lead to a variety of changes in the downstream river, including armoring of bed substrates, downcutting, changes to channel geometry, and vegetation encroachments (Kondolf & Matthews, 1991; Bunte, 2004; Harvey et al., 2005). These changes in morphology and sorting patterns can negatively impact fish populations, which rely on both the bed substrate and river morphology for spawning and habitat (Kondolf & Wolman, 1993; Harvey et al., 2005; May et al., 2009). Restoration efforts often seek to restore the sediment supply to the river to induce beneficial geomorphic and habitat changes in the form of reservoir sediment releases, dam removals, or gravel augmentation. The temporal and spatial manner in which these restoration measures elicit responses in the channel could have important consequences for the habitats that they seek to improve, and as our research shows, those changes could be temporary or permanent, and may take place at different times following the restoration activity. A better understanding of the persistence and temporal relationships of channel response to sediment supply changes can help guide restoration planning and project designs such that the range and duration of positive and negative impacts of those activities on aquatic habitat during critical life stages for aquatic species may be better foreseen.

5 Conclusion

We conducted a flume experiment to explore the response of a scaled fixed-wall gravel-bed meandering channel to a doubling in sediment supply. During our experiment, we observed multiple scales of simultaneous responses as the channel adjusted to an increase in sediment supply. Channel adjustments were observed to occur according to a timescale in proportion with the geomorphic work required; at a long enough time-scale, slope increase was the dominant response observed for our channel. The response of scaled gravel-dune bed forms and bar-pool morphology to increased sediment supply were observed to be transient and largely unaffected at each equilibrium condition during the experiment. This may indicate that gravel dunes and bar-pool morphology are not dependent on a specific sediment supply.

We characterized the relative influences of the observed responses using an total system resistance approach (Eaton & Church, 2004), which corroborated our observation that slope increase was the dominant mechanism by which the channel decreased long-term system resistance and increased transport capacity. We propose that this may be because the smaller spatial scale responses in our system had less response potential to reduce system resistance. A conceptual model for the response of a meandering channel to increases in sediment supply has been proposed to explain the observations seen in our experiment across spatial and temporal scales; the model acknowledges the importance of response potentials at each scale, as well as the implicit constraints on the channel that influence the overall system response. Further research is needed to better understand and quantify the response potentials for the various scales and types of responses for alluvial systems, as well as understand what drives the persistence some channel responses over others. Presently, this model provides a framework to reconcile the

variety of responses that have been observed in meandering channel studies experiencing sediment supply changes.

References

Bankert, A. R., & Nelson, P. A. (2018). Alternate bar dynamics in response to increases and decreases of sediment supply. *Sedimentology*, *65*(3), 702–720. https://doi.org/10.1111/sed.12399

Braudrick, C. A. (2013). *Meandering in Gravel-Bed Rivers* [UC Berkeley]. https://escholarship.org/uc/item/44h8s7b2

Brew, A. K., Morgan, J. A., & Nelson, P. A. (2015). Bankfull Width Controls on Riffle-pool Morphology Under Conditions of Increased Sediment Supply: Field Observations During the Elwha River Dam Removal Project. *Proceedings of the 3rd Joint Federal Interagency Conference on Sedimentation and Hydrologic Modeling*, 12.

Bridge, J. S. (1977). Flow, bed topography, grain size and sedimentary structure in open channel bends: A three-dimensional model. *Earth Surface Processes*, *2*(4), 401–416. https://doi.org/10.1002/esp.3290020410

Buffington, J. M. (2012). Changes in Channel Morphology Over Human Time Scales. In M. Church, P. M. Biron, & A. G. Roy (Eds.), *Gravel-Bed Rivers* (pp. 433–463). John Wiley & Sons, Ltd. https://doi.org/10.1002/9781119952497.ch32

Buffington, J. M., & Montgomery, D. R. (1999). Effects of sediment supply on surface textures of gravel-bed rivers. *Water Resources Research*, *35*(11), 3523–3530. https://doi.org/10.1029/1999WR900232

Bunte, K. (2004). *State of the Science Review Gravel Mitigation and Augmentation Below Hydroelectric Dams: A Geomorphological Perspective*. https://doi.org/10.13140/2.1.1094.3361

Bunte, K., & Abt, S. R. (2001). *Sampling surface and subsurface particle-size distributions in wadable gravel-and cobble-bed streams for analyses in sediment transport, hydraulics, and streambed monitoring* (RMRS-GTR-74; p. RMRS-GTR-74). U.S. Department of Agriculture, Forest Service, Rocky Mountain Research Station. https://doi.org/10.2737/RMRS-GTR-74

Carling, P. A. (1999). Subaqueous gravel dunes. *Journal of Sedimentary Research*, *69*(3), 534–545. https://doi.org/10.2110/jsr.69.534

Chang, H. H. (1979). Minimum stream power and river channel patterns. *Journal of Hydrology*, *41*(3), 303–327. https://doi.org/10.1016/0022-1694(79)90068-4

Clayton, J. A. (2010). Local sorting, bend curvature, and particle mobility in meandering gravel bed rivers. *Water Resources Research*, *46*(2). https://doi.org/10.1029/2008WR007669

Clayton, J. A., & Pitlick, J. (2007). Spatial and temporal variations in bed load transport intensity in a gravel bed river bend. *Water Resources Research*, *43*(2). https://doi.org/10.1029/2006WR005253

CloudCompare (2.8). (2020). [Computer software]. https://www.danielgm.net/cc/

Constantine, J., Dunne, T., Ahmed, J., Legleiter, C., & Lazarus, E. (2014). Sediment supply as a driver of river meandering and floodplain evolution in the Amazon Basin. *Nature Geosci*, *advance online publication*. https://doi.org/10.1038/ngeo2282

Cui, Y., Parker, G., Lisle, T. E., Gott, J., Hansler-Ball, M. E., Pizzuto, J. E., Allmendinger, N. E., & Reed, J. M. (2003). Sediment pulses in mountain rivers: 1. Experiments. *Water Resources Research*, *39*(9). https://doi.org/10.1029/2002WR001803

Davies, T. R. H., & Sutherland, A. J. (1983). Extremal hypotheses for river behavior. *Water Resources Research*, *19*(1), 141–148. https://doi.org/10.1029/WR019i001p00141

Dietrich, W. E., Kirchner, J. W., Ikeda, H., & Iseya, F. (1989). Sediment supply and the development of the coarse surface layer in gravel-bedded rivers. *Nature*, *340*(6230), 215–217. https://doi.org/10.1038/340215a0

Dietrich, W. E., & Smith, J. D. (1983). Influence of the point bar on flow through curved channels. *Water Resources Research*, *19*(5), 1173–1192. https://doi.org/10.1029/WR019i005p01173

Dietrich, W. E., & Whiting, P. (1989). Boundary Shear Stress and Sediment Transport in River Meanders of Sand and Gravel. In *River Meandering* (pp. 1–50). American Geophysical Union (AGU). https://doi.org/10.1029/WM012p0001

East, A. E., Pess, G. R., Bountry, J. A., Magirl, C. S., Ritchie, A. C., Logan, J. B., Randle, T. J., Mastin, M. C., Minear, J. T., Duda, J. J., Liermann, M. C., McHenry, M. L., Beechie, T. J., & Shafroth, P. B. (2015). Large-scale dam removal on the Elwha River, Washington, USA: River channel and floodplain geomorphic change. *Geomorphology*, *228*, 765–786. https://doi.org/10.1016/j.geomorph.2014.08.028

Eaton, B. C., & Church, M. (2004). A graded stream response relation for bed load–dominated streams. *Journal of Geophysical Research: Earth Surface*, *109*(F3). https://doi.org/10.1029/2003JF000062

Eaton, B. C., & Church, M. (2009). Channel stability in bed load–dominated streams with nonerodible banks: Inferences from experiments in a sinuous flume. *Journal of Geophysical Research: Earth Surface*, *114*(F1). https://doi.org/10.1029/2007JF000902

Erwin, S. O. (2013). *Development of sediment budgets at multiple scales*. 179.

Gilbert, G. K. (1917). Hydraulic-mining debris in the Sierra Nevada. *Professional Paper*, Article 105. https://doi.org/10.3133/pp105

Harvey, B., McBain, S., Reiser, D., Rempel, L., Sklar, L. S., & Lave, R. (2005). *Key uncertainties in Gravel Augmentation: Geomorphological and Biological Research Needs for Effective River Restoration* (CALFED Science Program and Ecosystem Restoration Program Gravel Augmentation Panel Report, pp. 1–99).

Huang, H. Q., & Nanson, G. C. (2000). Hydraulic geometry and maximum flow efficiency as products of the principle of least action. *Earth Surface Processes and Landforms*, *25*(1), 1–16. https://doi.org/10.1002/(SICI)1096-9837(200001)25:1<1::AID-ESP68>3.0.CO;2-2

Ingle, J. (1966). *The Movement of Beach Sand: An Analysis Using Fluorescent Grains*. Elsevier.

Kleinhans, M. G. (2005). Phase diagrams of bed states in steady, unsteady, oscillatory and mixed flows. In *EU-Sandpit end-book, Ed. Leo van Rijn* P*aper Q.* Aqua Publications, The Netherlands

Kondolf, G. M., & Matthews, W. V. G. (1991). *Management of Coarse Sediment in Regulated Rivers of California*. https://escholarship.org/uc/item/5rw9k19j

Kondolf, G. M., & Wolman, M. G. (1993). The sizes of salmonid spawning gravels. *Water Resources Research*, *29*(7), 2275–2285. https://doi.org/10.1029/93WR00402

Lane, E. W. (1955). The importance of fluvial morphology in hydraulic engineering. *Proceedings of the American Society of Civil Engineers*, *81*(7), 1–17.

Langbein, W. B., & Leopold, L. B. (n.d.). *River Meanders Theory of Minimum Variance*. 21. https://doi.org/10.3133/pp422h

Legleiter, C. J., & Kyriakidis, P. C. (2007). Forward and Inverse Transformations between Cartesian and Channel-fitted Coordinate Systems for Meandering Rivers. *Mathematical Geology*, *38*(8), 927–958. https://doi.org/10.1007/s11004-006-9056-6

Lisimenka, A., & Kubicki, A. (2017). Estimation of dimensions and orientation of multiple riverine dune generations using spectral moments. *Geo-Marine Letters*, *37*(1), 59–74. https://doi.org/10.1007/s00367-016-0475-1

Lisle, T. (1982). Effects of aggradation and degradation on riffle-pool morphology in natural gravel channels, northwestern California. *Water Resources Research*, *18*(6), 1643–1651. https://doi.org/10.1029/WR018i006p01643

Lisle, T., & Hilton, S. (1992). The Volume of Fine Sediment in Pools: An Index of Sediment Supply in Gravel-Bed Streams1. *JAWRA Journal of the American Water Resources Association*, *28*(2), 371–383. https://doi.org/10.1111/j.1752-1688.1992.tb04003.x

Lisle, T., Iseya, F., & Ikeda, H. (1993). Response of a Channel with alternate bars to a decrease in supply of mixed-size bed load: A Flume Experiment. *Water Resources Research*, *29*(11), 3623–3629. https://doi.org/10.1029/93WR01673

Lisle, T., & Madej, M. A. (1992). Spatial variation in armouring in a channel with high sediment supply. *In: P. Billi, R.D. Hey, C.R. Thorne, and P. Tacconi (Ed.), Dynamics of Gravel-Bed Rivers. John Wiley and Sons, London. p. 277-293.* https://www.fs.usda.gov/treesearch/pubs/7829

Mackin, J. (1948). Concept of the Graded River. *Bulletin of The Geological Society of America*, *59*, 463–512. https://doi.org/10.1130/0016-7606(1948)59[463:COTGR]2.0.CO;2

Madej, M. A. (2001). Development of channel organization and roughness following sediment pulses in single-thread, gravel bed rivers. *Water Resources Research*, *37*(8), 2259–2272. https://doi.org/10.1029/2001WR000229

Marion, A., & Fraccarollo, L. (1997). New Conversion Model for Areal Sampling of Fluvial Sediments. *Journal of Hydraulic Engineering*, *123*(12), 1148–1151. https://doi.org/10.1061/(ASCE)0733-9429(1997)123:12(1148)

Mark, C. F. van der, Blom, A., & Hulscher, S. J. M. H. (2008). Quantification of variability in bedform geometry. *Journal of Geophysical Research: Earth Surface*, *113*(F3). https://doi.org/10.1029/2007JF000940

May, C. L., Pryor, B., Lisle, T. E., & Lang, M. (2009). Coupling hydrodynamic modeling and empirical measures of bed mobility to predict the risk of scour and fill of salmon redds in a large regulated river. *Water Resources Research*, *45*(5). https://doi.org/10.1029/2007WR006498

Millar, R. G. (1999). Grain and form resistance in gravel-bed rivers Résistances de grain et de forme dans les rivières à graviers. *Journal of Hydraulic Research*, *37*(3), 303–312. https://doi.org/10.1080/00221686.1999.9628249

Morgan, J. A. (2018). *The effects of sediment supply, width variations, and unsteady flow on riffle-pool dynamics*. 203.

Morgan, J. A., Brogan, D. J., & Nelson, P. A. (2017). Application of Structure-from-Motion photogrammetry in laboratory flumes. *Geomorphology*, *276*, 125–143. https://doi.org/10.1016/j.geomorph.2016.10.021

Nelson, P. A., Brew, A. K., & Morgan, J. A. (2015). Morphodynamic response of a variable-width channel to changes in sediment supply. *Water Resources Research*, *51*(7), 5717–5734. https://doi.org/10.1002/2014WR016806

Nelson, P. A., Dietrich, W. E., & Venditti, J. G. (2010). Bed topography and the development of forced bed surface patches. *Journal of Geophysical Research: Earth Surface*, *115*(F4). https://doi.org/10.1029/2010JF001747

Nelson, P. A., & Morgan, J. A. (2018). Flume experiments on flow and sediment supply controls on gravel bedform dynamics. *Geomorphology*, *323*, 98–105. https://doi.org/10.1016/j.geomorph.2018.09.011

Nelson, P. A., Venditti, J. G., Dietrich, W. E., Kirchner, J. W., Ikeda, H., Iseya, F., & Sklar, L. S. (2009). Response of bed surface patchiness to reductions in sediment supply. *Journal of Geophysical Research: Earth Surface*, *114*(F2). https://doi.org/10.1029/2008JF001144

Nikuradse, J. (1933). *Laws of flow in rough pipes*. National Advisory Committee for Aeronautics; WorldCat.org.

Parker, G. (1990). Surface-based bedload transport relation for gravel rivers. *Journal of Hydraulic Research*, *28*(4), 417–436. https://doi.org/10.1080/00221689009499058

Parker, Gary, & Andrews, E. D. (1985). Sorting of Bed Load Sediment by Flow in Meander Bends. *Water Resources Research*, *21*(9), 1361–1373. https://doi.org/10.1029/WR021i009p01361

Parker, Gary, Toro-Escobar, C. M., Ramey, M., & Beck, S. (2003). Effect of Floodwater Extraction on Mountain Stream Morphology. *Journal of Hydraulic Engineering*, *129*(11), 885–895. https://doi.org/10.1061/(ASCE)0733-9429(2003)129:11(885)

Perron, J. T., Kirchner, J. W., & Dietrich, W. E. (2008). Spectral signatures of characteristic spatial scales and nonfractal structure in landscapes. *Journal of Geophysical Research*, *113*(F4), F04003. https://doi.org/10.1029/2007JF000866

Pitlick, J. (1992). Flow resistance under conditions of intense gravel transport. *Water Resources Research*, *28*(3), 891–903. https://doi.org/10.1029/91WR02932

Podolak, C. J. P., & Wilcock, P. R. (2013). Experimental study of the response of a gravel streambed to increased sediment supply. *Earth Surface Processes and Landforms*, *38*(14), 1748–1764. https://doi.org/10.1002/esp.3468

Rathburn, S., & Wohl, E. (2003). Predicting fine sediment dynamics along a pool-riffle mountain channel. *Geomorphology*, *55*(1), 111–124. https://doi.org/10.1016/S0169-555X(03)00135-1

Schumm, S. A. (1968). Speculations Concerning Paleohydrologic Controls of Terrestrial Sedimentation. *GSA Bulletin*, *79*(11), 1573–1588. https://doi.org/10.1130/0016-7606(1968)79[1573:SCPCOT]2.0.CO;2

Smith, J. D., & Mclean, S. R. (1984). A Model for Flow in Meandering Streams. *Water Resources Research*, *20*(9), 1301–1315. https://doi.org/10.1029/WR020i009p01301

Southard, J. B., & Boguchwal, L. A. (1990). Bed configuration in steady unidirectional water flows; Part 2, Synthesis of flume data. *Journal of Sedimentary Research*, *60*(5), 658–679. https://doi.org/10.1306/212F9241-2B24-11D7-8648000102C1865D

USGS. (2017). *Unmanned Aircraft Systems Data Post Processing Structure from Motion Photogrammetry*. USGS National UAS Project Office.

van Dijk, T. A. G. P., Lindenbergh, R. C., & Egberts, P. J. P. (2008). Separating bathymetric data representing multiscale rhythmic bed forms: A geostatistical and spectral method compared. *Journal of Geophysical Research*, *113*(F4), F04017. https://doi.org/10.1029/2007JF000950

Venditti, J. G., Dietrich, W. E., Nelson, P. A., Wydzga, M. A., Fadde, J., & Sklar, L. (2010a). Effect of sediment pulse grain size on sediment transport rates and bed mobility in gravel bed rivers. *Journal of Geophysical Research: Earth Surface*, *115*(F3). https://doi.org/10.1029/2009JF001418

Venditti, J. G., Dietrich, W. E., Nelson, P. A., Wydzga, M. A., Fadde, J., & Sklar, L. (2010b). Mobilization of coarse surface layers in gravel-bedded rivers by finer gravel bed load. *Water Resources Research*, *46*(7). https://doi.org/10.1029/2009WR008329

Venditti, J. G., Nelson, P. A., Bradley, R. W., Haught, D., & Gitto, A. B. (2017). Bedforms, Structures, Patches, and Sediment Supply in Gravel-Bed Rivers. In *Gravel-Bed Rivers* (pp. 439–466). John Wiley & Sons, Ltd. https://doi.org/10.1002/9781118971437.ch16

Venditti, J. G., Nelson, P. A., Minear, J. T., Wooster, J., & Dietrich, W. E. (2012). Alternate bar response to sediment supply termination: ALTERNATE BARS AND SEDIMENT SUPPLY. *Journal of Geophysical Research: Earth Surface*, *117*(F2), n/a-n/a. https://doi.org/10.1029/2011JF002254

Wang, L., Yu, Q., & Gao, S. (2019). *A combined method to calculate superimposed 2-D dune morphological parameters*. Marine and River Dune Dynamics - MARID VI, Bremen, Germany.

Wang, L., Yu, Q., Zhang, Y., Flemming, B. W., Wang, Y., & Gao, S. (2020). An automated procedure to calculate the morphological parameters of superimposed rhythmic bedforms. *Earth Surface Processes and Landforms*, esp.4983. https://doi.org/10.1002/esp.4983

Whiting, P. J., & Dietrich, W. E. (1991). Convective accelerations and boundary shear stress over a Channel Bar. *Water Resources Research*, *27*(5), 783–796. https://doi.org/10.1029/91WR00083

Wilcock, P. R., & Crowe, J. (2003). Surface-based Transport Model for Mixed-Size Sediment. *Journal of Hydraulic Engineering*, *129*(2), 120–128. https://doi.org/10.1061/(ASCE)0733-9429(2003)129:2(120)

Wilcock, P. R., & McArdell, B. W. (1993). Surface-based fractional transport rates: Mobilization thresholds and partial transport of a sand-gravel sediment. *Water Resources Research*, *29*(4), 1297–1312. https://doi.org/10.1029/92WR02748

Williams, G. P., & Wolman, M. G. (1984). Downstream effects of dams on alluvial rivers. *United States Geological Survey Professional Paper*, *1286*, 83.

Wohl, E. E., & Cenderelli, D. A. (2000). Sediment deposition and transport patterns following a reservoir sediment release. *Water Resources Research*, *36*(1), 319–333. https://doi.org/10.1029/1999WR900272

Wolman, M. G., & Miller, J. P. (1960). Magnitude and Frequency of Forces in Geomorphic Processes. *The Journal of Geology*, *68*(1), 54–74. https://doi.org/10.1086/626637

Young, D. (2020). *Fourier transform demonstration*. MATLAB Central File Exchange. https://www.mathworks.com/matlabcentral/fileexchange/28810-fourier-transform-demonstration

Appendix A

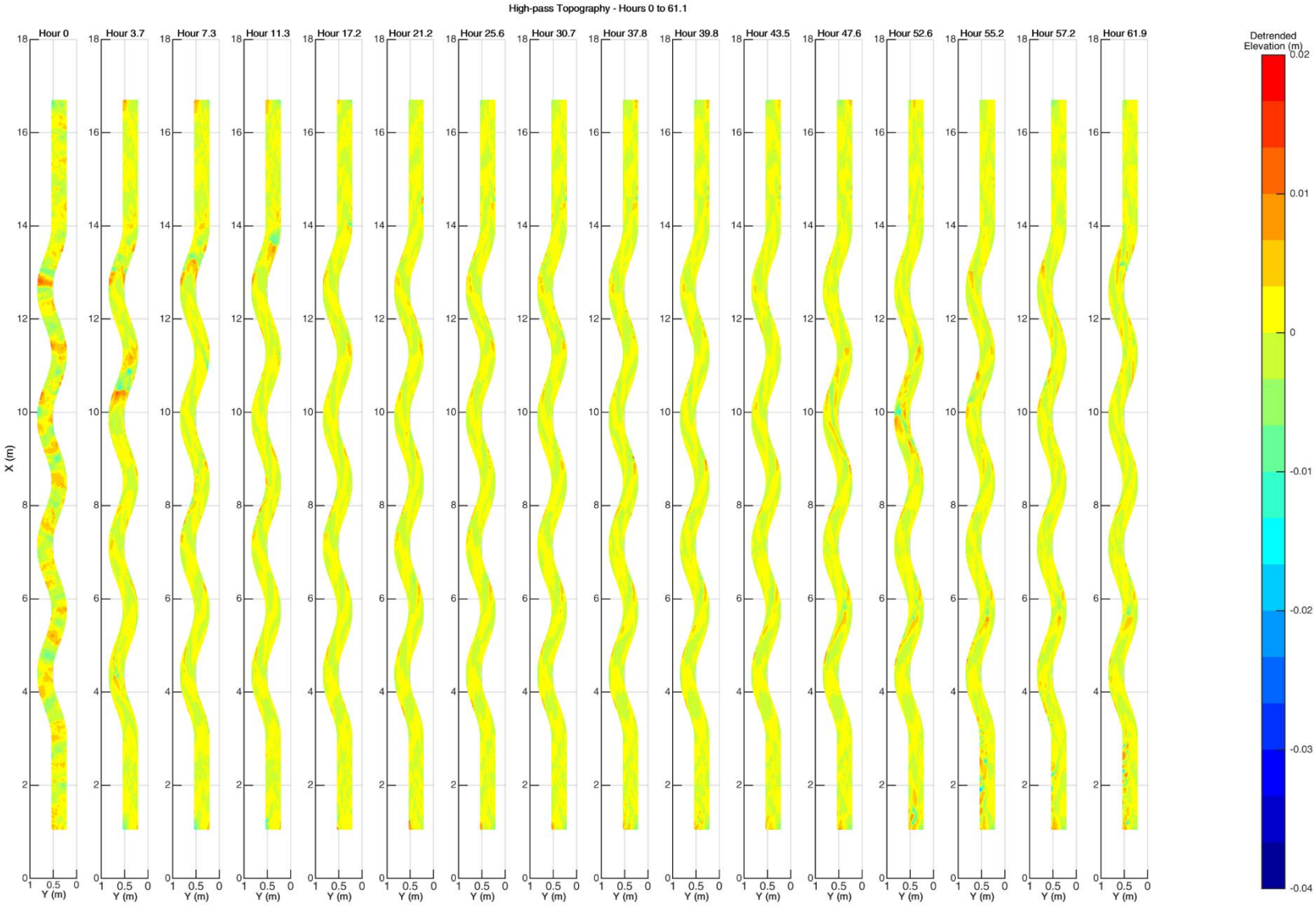

Figure A1a High-pass topographic data for 0 hrs to 61.9 hrs.

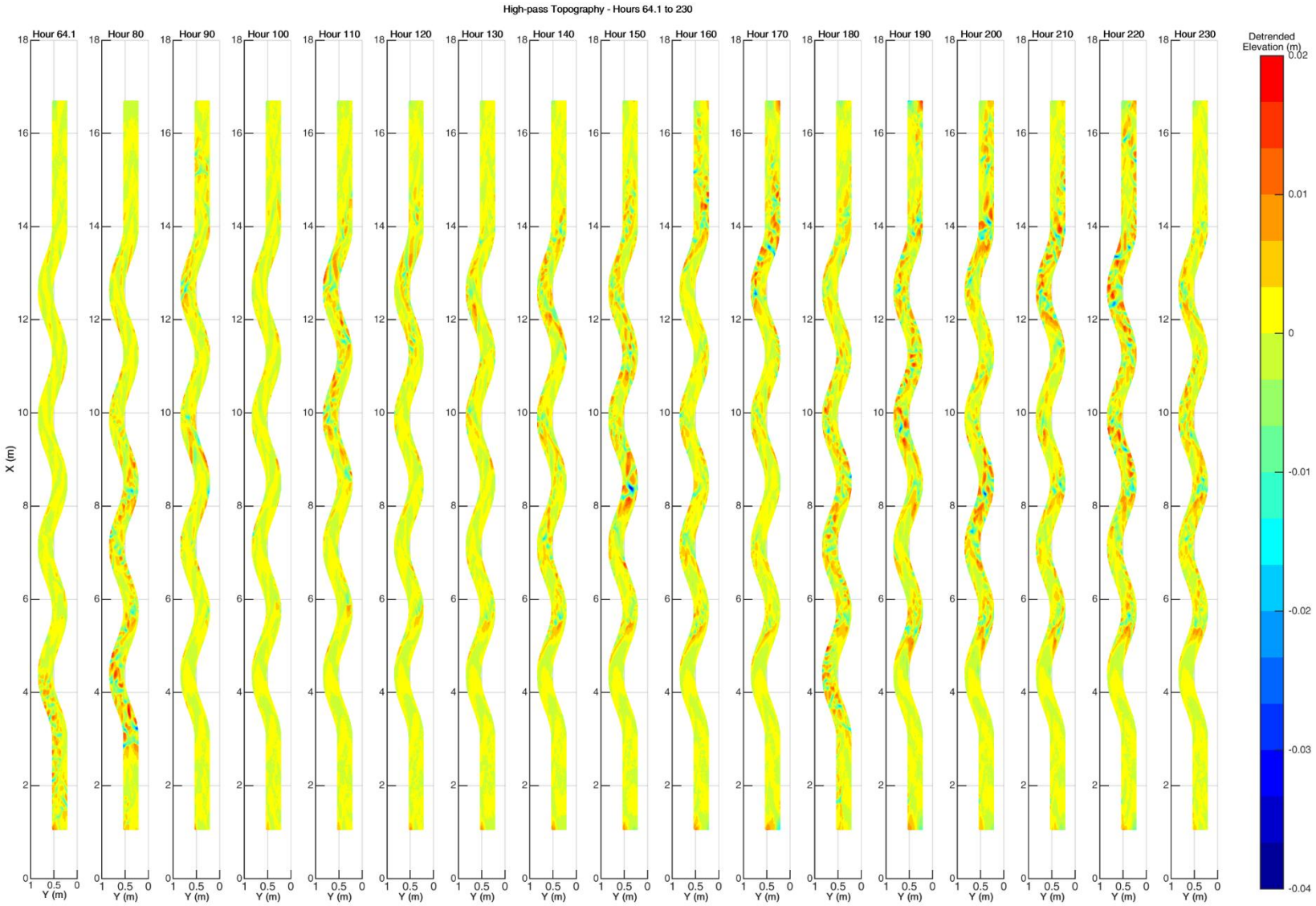

Figure A1b High-pass topographic data for 64.1 hrs to 230.1 hrs.

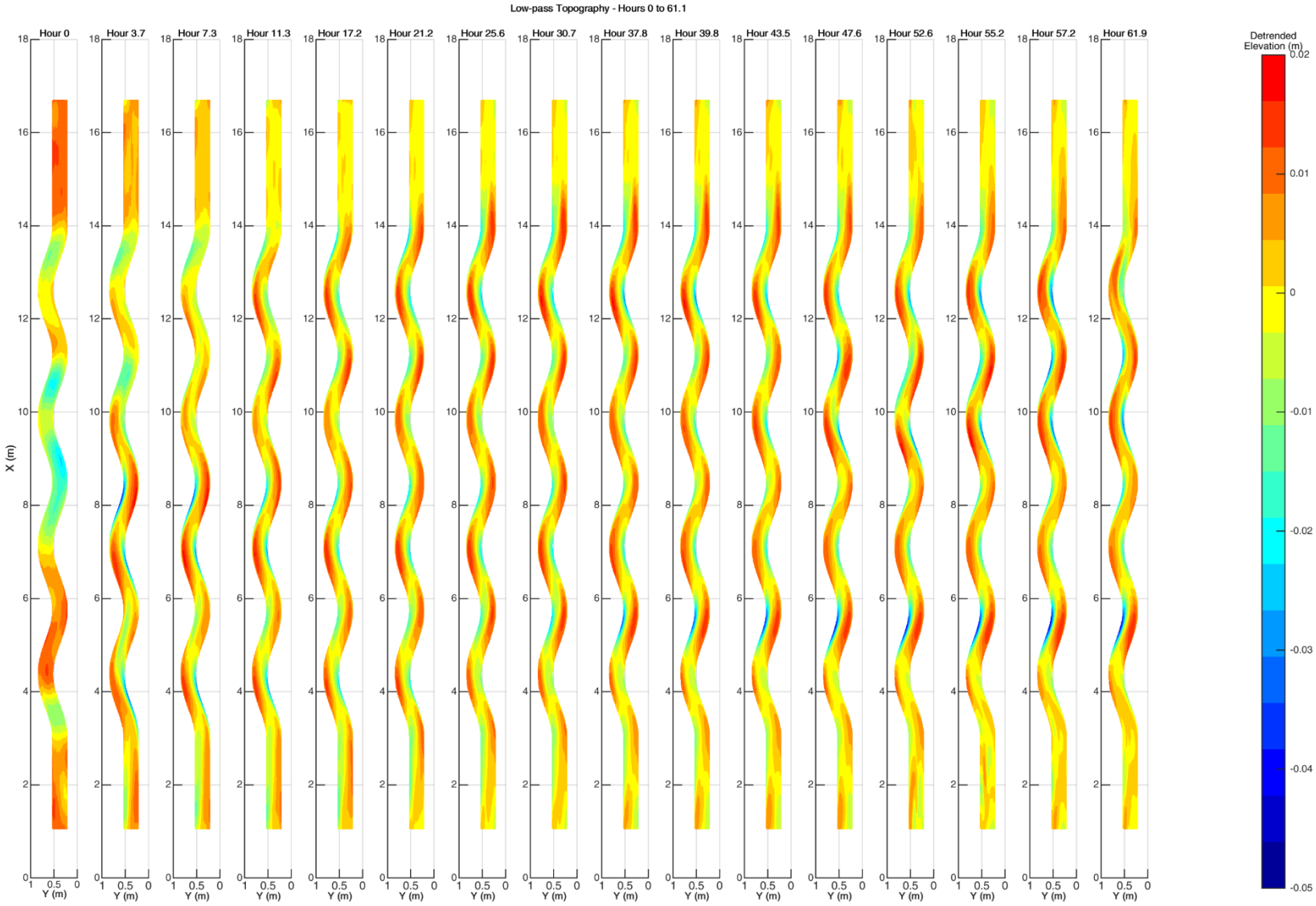

Figure A2a Low-pass topographic data for 0 hrs to 61.9 hrs.

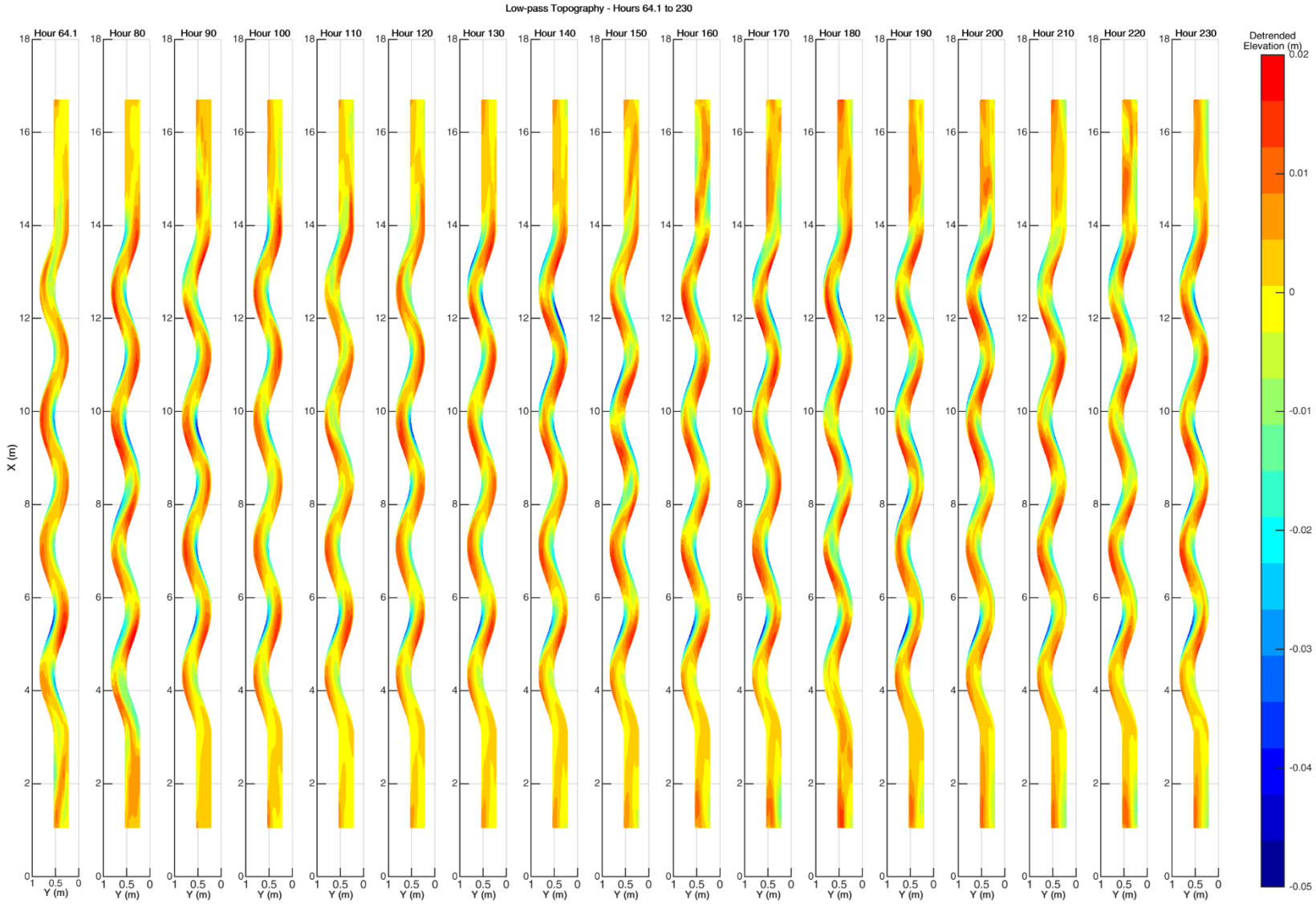

Figure A2b Low-pass topographic data for 64.1 hrs to 230.1 hrs.

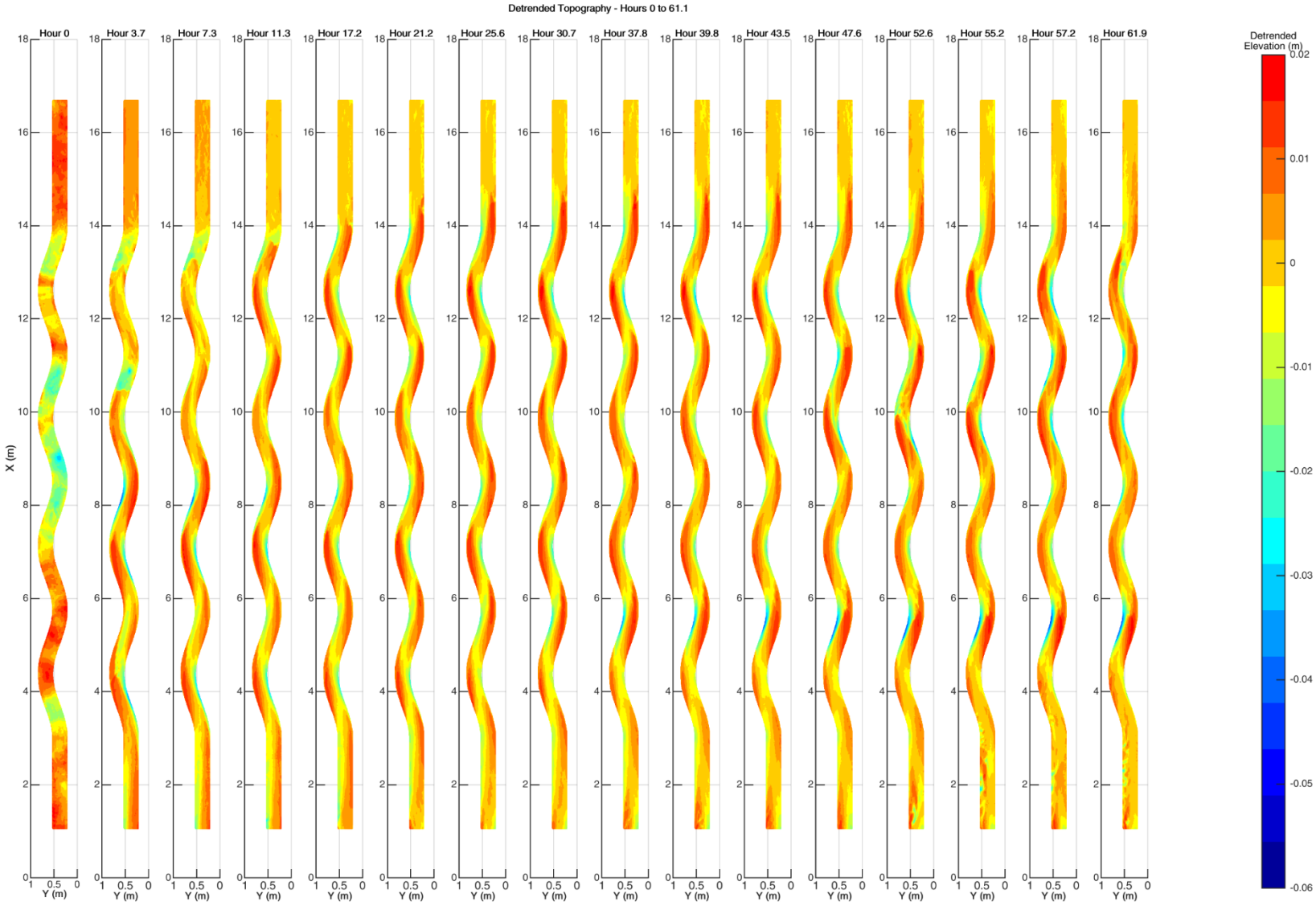

Figure A3a Detrended topographic data for 0 hrs to 61.9 hrs.

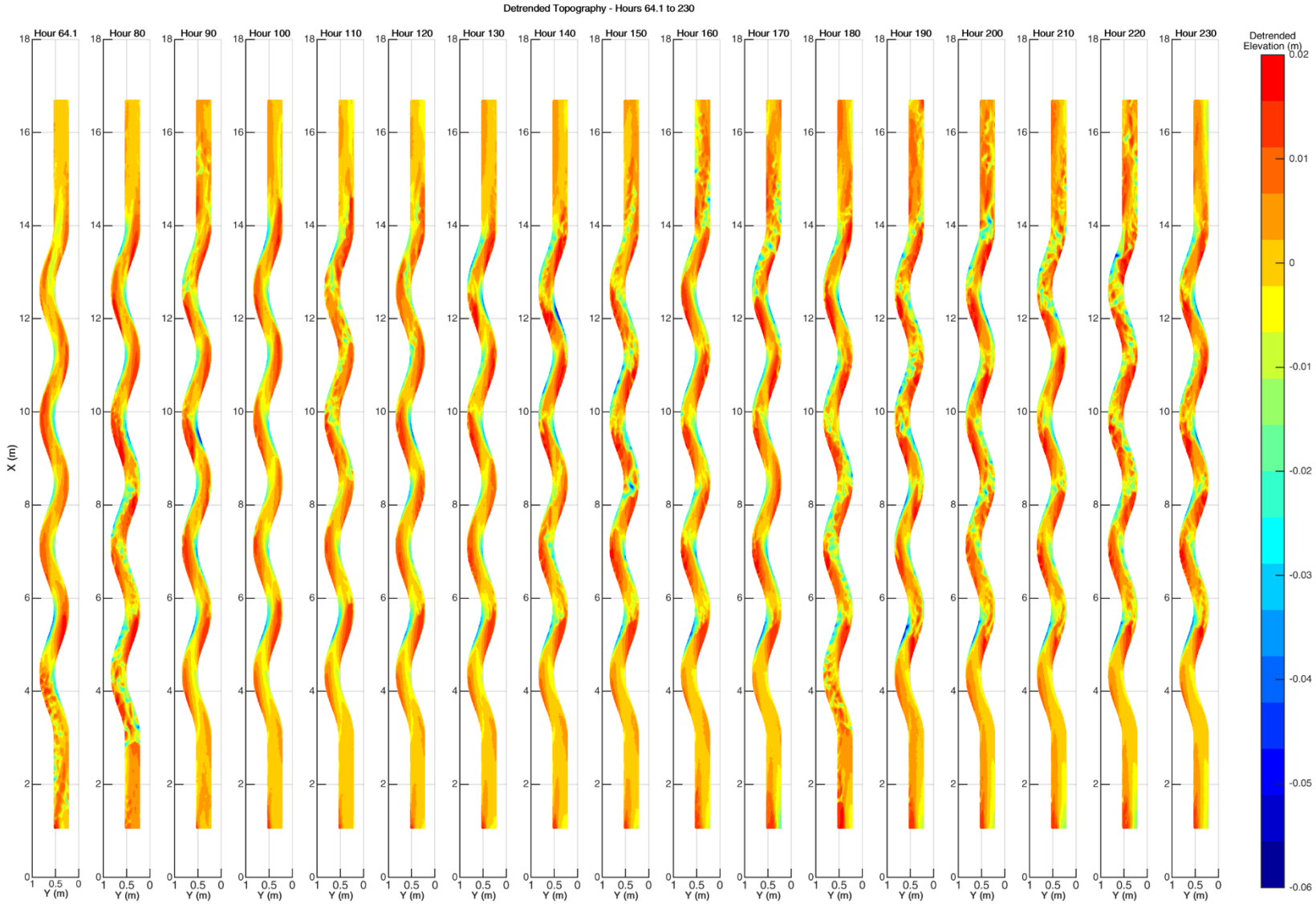

Figure A3b Detrended topographic data for 64.1 hrs to 230.1 hrs.